Article type: Progress Report

Title: Perovskite solar cells with ZnO electron transporting materials

Peng Zhang, Jiang Wu, Ting Zhang, Yafei Wang, Detao Liu, Hao Chen, Long Ji, Chunhua Liu, Waseem Ahmad, Zhi David Chen and Shibin Li**

Dr. Peng Zhang, Dr. Ting Zhang, Dr. Yafei Wang, Dr. Detao Liu, Dr. Hao Chen, Dr. Long Ji, Dr. Chunhua Liu, Dr. Waseem Ahmad, Prof. Shibin Li

School of Optoelectronic Information

University of Electronic Science and Technology of China

Chengdu 610054, China.

E-mail: shibinli@uestc.edu.cn

Dr. Jiang Wu

Department of Electronic and Electrical Engineering

University College London

Torrington Place, London WC1E7JE, UK.

E-mail: jiang.wu@ucl.ac.uk

Prof. Zhi David Chen

Department of Electrical & Computer Engineering and Center for Nanoscale Science & Engineering

University of Kentucky

Lexington, Kentucky 40506, USA.

Keywords

perovskite solar cells, zinc oxide, electron transport materials, nanostructures, photovoltaics

Abstract

Perovskite solar cells (PSCs) have been developed rapidly over the past few years, and the power conversion efficiency (PCE) of PSCs has exceeded 20%. Such high performance can be attributed to the unique properties, such as high absorption over visible range and long diffusion length, of perovskite materials. Due to the different diffusion length of holes and electrons, electron transporting material (ETM) used in PSCs plays a critical role in PSCs performance. As an alternative to TiO_2 ETM, ZnO materials have similar physical properties to TiO_2 but with much higher electron mobility. In addition, there are many simple and facile methods to fabricate ZnO nanomaterials with low cost and energy consumption. This review focuses on recent developments in the use of ZnO ETM for PSCs. The fabrication methods of ZnO materials are briefly introduced. The influence of different ZnO ETMs on performance of PSCs is then reviewed. The limitations of ZnO ETM based PSCs and some solutions to these challenges are also discussed. The review provides a systematic and comprehensive understanding of the influence of different ZnO ETMs on PSCs performance and potentially motivates further development of PSCs by extending the knowledge of ZnO based PSCs to TiO_2 based PSCs.

1. Introduction

Organic-inorganic hybrid perovskite materials are one of the most promising candidates for high efficient and low-cost solar cells. The typical chemical formula of perovskite compounds is ABX_3, as shown in **Figure 1**(a), where A stands for an organic cation or organic cation group, like Cs^+, $CH_3NH_3^+$(MA), or $NH{=}CHNH^{3+}$(FA), B is an inorganic cation, e.g. Pb^{2+} or Sn^{2+}, and X stands for a halogen ion, such as I, Cl and Br.[1-10]

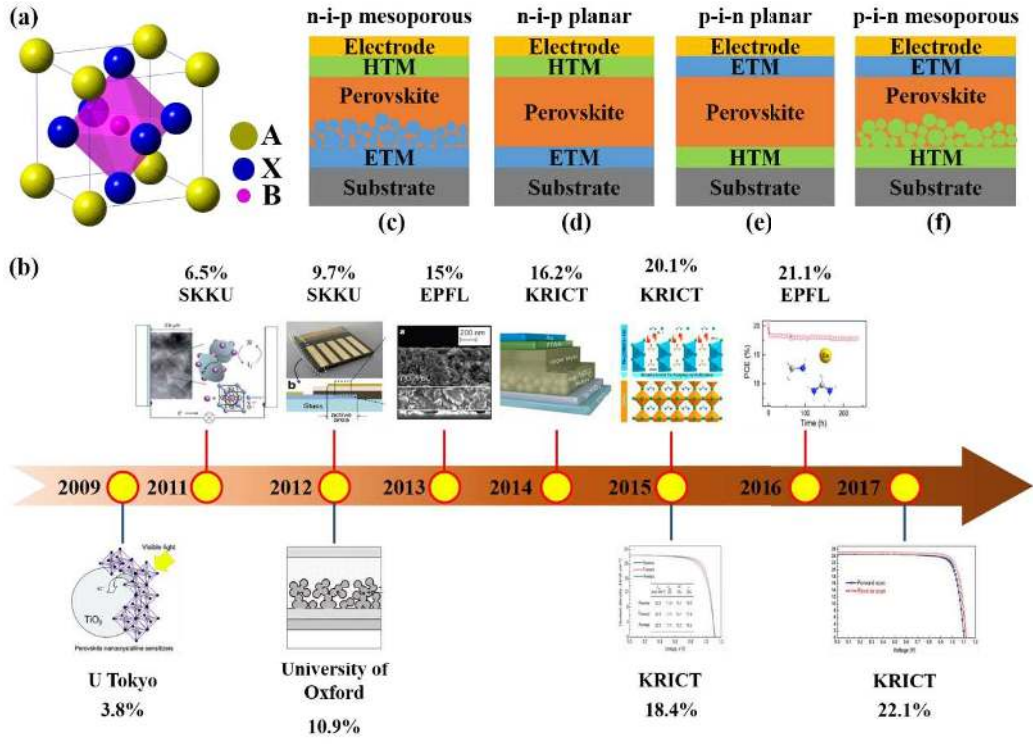

Figure 1. (a) The crystal structure of organic-inorganic hybrid perovskites, where A = cation or organic cation group, B = Pb^{2+} or Sn^{2+} and X = halogen ion. (b) The development history of PSCs. (c) - (f) the typical structures of PSCs: (c) n-i-p mesoporous structure; (d) n-i-p planar structure; (e) p-i-n planar structure; (f) p-i-n mesoporous structure.

Compared to an ordinary organic semiconductor or inorganic semiconductor, the organic-inorganic hybrid perovskite shows unique electrical properties and optical properties. Firstly, hybrid perovskite materials have a larger Bohr radius,[11] a high dielectric constant and a weak exciton binding energy,[12, 13] which mean light induced excitons will dissociate into free carriers quickly at room temperature. Secondly, perovskite materials have a long carrier diffusion length and high carrier diffusion velocity.[14-20] Thirdly, the most used perovskite materials have a band gap of about 1.5 eV, which makes it an excellent light absorber in the UV-Vis range.[11] All these advantages mentioned above show that organic-inorganic hybrid perovskite materials have a great potential in photovoltaics and potentially beyond.[21]

In 2009, $MAPbBr_3$ nanocrystalines were first introduced into a dye-sensitized solar cell (DSSC) as a sensitizer by Kojima et al., and the PCE of the perovskite sensitized solar cell was 3.8%.[22] In 2011, by improving the quality of mesoporous TiO_2 ETM and using $MAPbI_3$ quantum dots (QDs) as the sensitizer, Im et al. increased the PCE of a PSC to 6.5%.[23] However, both their solar cells show poor stability due to the use of liquid electrolytes. The liquid electrolyte gradually dissolves perovskite under irradiation, which seriously degrades solar cell performance. In 2012, Kim et al. replaced the liquid electrolyte with a solid hole transporting material (HTM), spiro-MeOTAD. The solid HTM dramatically improved the stability and efficiency of the PSC, and the all solid solar cell yields a PCE of 9.7%.[24] In 2013, Burschka et al. replaced the traditional single step method with a novel sequential deposition method and they obtained a high quality $MAPbI_3$ film. The films from different batches have

similar properties and deviation of solar cell performances is relatively small, which show the good reproducibility of this method.[25] By using this method, the PCE of the PSCs soared to about 15%. In 2014, Zhou et al. used polyethyleneimine ethoxylated (PEIE) and Y doped TiO_2 to modify the carrier extraction process at the electrode, and combined with a composite $MAPbI_{3-x}Cl_x$ perovskite material, the PCE of their solar cell boosted to 19.3%.[26]

Besides the methylammonium lead halide ($MAPbI_3$) materials, formamidinium lead iodide ($FAPbI_3$) is another promising perovskite material. $FAPbI_3$ has more suitable bandgap but poor stability.[27] In 2015, Jeon et al. stabilized the $FAPbI_3$ by incorporating $MAPbBr_3$ into $FAPbI_3$, and their strategy promoted the PCE of $FAPbI_3$ based solar cells from 4.3% to more than 18%.[28-34] On the basis of Jeon's work, through an intramolecular exchange method, Yang et al. fabricated a high quality perovskite film by increasing the crystallization properties of the $(FAPbI_3)_{1-x}(MAPbBr_3)_x$, and a maximum PCE of 20.2% was obtained.[35] Almost at the same time, Bi et al. increased the PCE to 20.8% by suppressing the recombination through residual PbI_2 in the perovskite film.[36] Recently, Saliba et al. provided a novel method to fabricate a PSC based on perovskite material with all three cations, Cs, MA, and FA.[37] Through this method, they obtained a stable solar cell with a high PCE of 21.1%. The latest record PCE had been reported by Yang et al. In their research, $(FAPbI_3)_{1-x}(MAPbBr_3)_x$ was synthesized by an intramolecular exchanging process and additional iodide ions were introduced into perovskite to decrease the defects, and a record high PCE of 22.1% was obtained.[38] The brief development history of PSCs is displayed in

Figure 1(b).

Based on the unique properties of perovskite materials, two kinds of device structures are usually used: mesoporous structure and planar structure. Both structures further contains two different types: the n-i-p type and p-i-n type. The schematic device structures are exhibited in Figure 1(c)-(f). The ETM here is used to compensate and balance the difference of hole and electron diffusion lengths.[12] In addition, the ETM is a blocking layer that prevents holes from reaching the FTO electrode. For high performance solar cells, ETMs should meet the following criteria: (a) good optical transmittance in the visible range, which reduces the optical energy loss; (b) the energy levels of ETMs should match that of perovskite materials, which improve the electron extraction efficiency and block holes; (c) good electron mobility; (d) a high quality ETM film can be easy to obtain in terms of fabrication. As a result, the design and materials properties of the ETM are crucial for solar cell performance.[11-13, 39]

TiO_2 is the most widely used ETM for PSCs. The proper band gap and high transmittance of TiO_2 guarantee the high performance of solar cells. However, to obtain a high quality compact or mesoporous TiO_2 film, high temperature annealing is unavoidable under most conditions, which restricts its application in flexible devices and increases the production cost. Additionally, electron mobility of perovskite materials is about 7.5 $cm^2V^{-1}s^{-1}$ and that of TiO_2 is in the range of 0.1 - 4 $cm^2V^{-1}s^{-1}$. The lower electron mobility in TiO_2 may cause the degradation of solar cell performance.[40]

Besides the TiO_2 ETM, organic conducting materials, such as the fullerene and its derivatives have also been widely used as the ETM in PSCs.[41-50] Collavini et al.

prepared PSCs based on the C70 and C60 ETM through a novel solution process. By using this method, the PCE of PSCs based on the C70 and C60 ETM were 10.4% and 11.4%, respectively.[51] On the basis of these works, Pascual et al. fabricated PSCs based on $MAPbI_3$-C70 blend without any extra ETM. A PCE of 13.6% was obtained based on this simple and efficient structure.[52] Besides the pristine fullerene, the fullerene derivative [6,6]-phenyl C61 butyric acid methyl ester (PCBM) is also widely used as the ETM in PSCs. PCBM inherits the high electron mobility of fullerenes and shows a good solubility due to the introduction of organic groups. Usually, Poly(3,4-ethylenedioxythiophene) Polystyrene sulfonate (PEDOT:PSS) and PCBM are used together as the HTM and ETM in PSCs respectively. Based on this group, a great deal of researches have been carried out. Docampo et al. fabricated planar-heterojunction PSCs, which obtained a PCE of 10% on glass substrates and over 6% on flexible polymer substrates.[53] Wu et al. obtained efficient invert PSCs with a PCE of 18% by using a small amount of H_2O as an additive to the perovskite precursor solution.[54] Following this work, Chiang et al. fabricated a high quality thick $MAPbI_3$ film with large grain sizes through the use of H_2O additives and DMF vapor treatment during the two-step spin coating process. Based on this modified two-step process, a high PCE of 20.1% was obtained.[55] As can be seen, the fullerene and its derivatives are also efficient ETM for PSCs, the performance of PSCs based on fullerene derivatives is comparable to that of TiO_2 based PSCs. Furthermore, high quality fullerene and its derivatives can be fabricated by low temperature solution process, which is favorable to reduce the cost. However, electron mobility in C60 film is about 1 $cm^2V^{-1}s^{-1}$ and

that of PCBM is 2.6×10^{-4} $cm^2V^{-1}s^{-1}$, both of which are lower than that of TiO_2.[56,57] On the other hand, the position of valence band of fullerene and its derivatives (-6.3 eV for C60, -6.0 eV for PCBM, compared with vacuum energy level) is higher than that of TiO_2 (-8.0 eV, compared with vacuum energy level), which lead to a weaker hole blocking ability.[58,59] Additionally, according to the research of Bao et al., the fullerene part of PCBM molecules interacts with oxygen and water, which results in device degradation.[60]

ZnO is another widely used ETM, which has attracted much attention as an alternative to TiO_2 in DSSCs and polymer solar cells. Recently, ZnO based PSCs have also been researched systematically. Although the best PCE of ZnO based PSCs is about 17%, which is inferior to that of TiO_2 based PSCs, ZnO is still the an efficient and promising alternative to TiO_2 in PSCs.[61] First of all, ZnO has very high transmittance in the visible spectra and more importantly, is low in cost. As shown in **Figure 2**(a) and (b), ZnO has similar energy band position and physical properties to TiO_2 but much higher electron mobility, which can potentially improve the electron transport efficiency and reduce the recombination loss as an ETM.[62-64] Secondly, ZnO is easy to crystallize and dope. At the same time, the layered structure of ZnO crystal structure, like shown in Figure 2(c), lead to a different growth rates along different directions, as a result, various ZnO nanostructures, such like nanowires,[65-67] nanotubes,[68,69] nanobelts,[70-72] nanorings,[73-75] nanoflowers,[76-78] nanorods and so on,[79,80] can be fabricated easily. Last but not least, high temperature annealing is not necessary for most ZnO fabrication methods, which means that it can be produced with a lower cost

and thermal budget and thus be potentially used in flexible devices. These properties make ZnO a promising ETM for PSCs. Meanwhile, although most physical properties of ZnO and TiO_2 are similar, there are also some distinct properties for each material. As a result, studies on ZnO based solar cells enrich the family of PSCs, which will in turn help to improve the performance of PSCs.

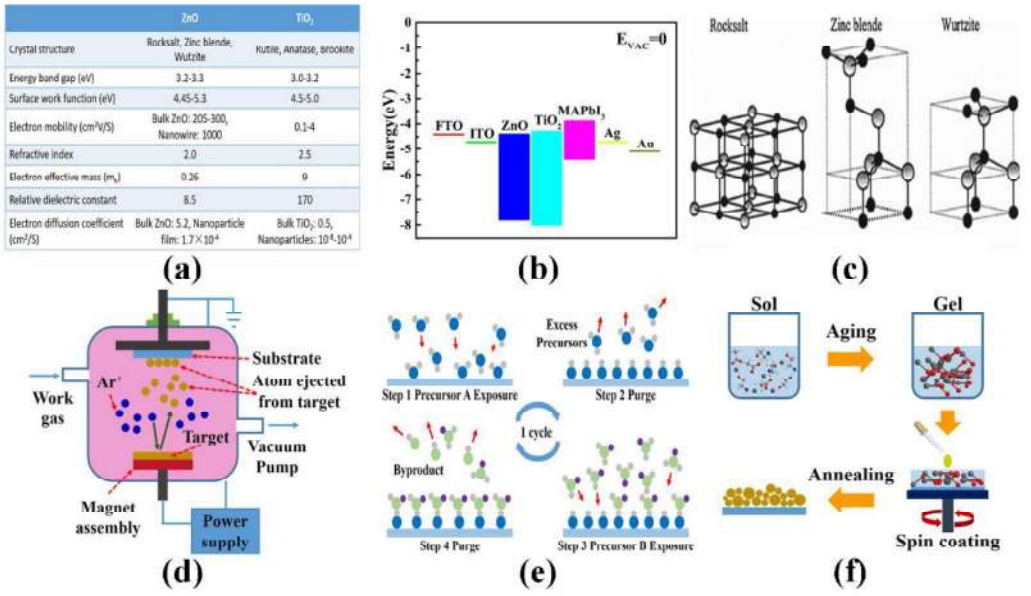

Figure 2. (a) Comparison of the electrical properties of ZnO and TiO_2.[61-63] (b) The energy level of ZnO, TiO_2 and other usually used materials in PSCs.[63] (c) Three different crystal structures of ZnO. Schematics of the usually used ZnO synthesis methods: (d) RF sputtering, (e) atomic layer deposition and (f) sol-gel method.

In this article, we briefly summarized the common fabrication methods of ZnO materials and systematically reviewed the application of various types of ZnO ETMs in PSCs. The review shows the origin of different performances between ZnO ETM based PSCs and TiO_2 based PSCs. The important role of ZnO ETM preparation and optimization in solar cell performance is introduced. In addition, limitations of ZnO

ETMs are also discussed. This review tends to present a timely update on the recent development of ZnO ETM based PSCs and provides some guidelines for further optimization and design of PSCs based on ZnO ETMs and beyond.

2. Planar PSCs with a compact ZnO film as the ETM

As well known, perovskite materials have a long carrier diffusion length and ambipolar behavior. In other words, perovskite materials can efficiently transport both electrons and holes. This indicates that planar structure PSC is feasible. A simpler solar cell structure without the mesoporous layer opens opportunities for potential applications of PSCs in tandem solar cell and flexible devices. Thanks to the high mobility of ZnO, to date, planar PSCs with a compact ZnO film as the ETM have been widely studied.

To achieve high performance PSCs, a uniform and thin ZnO film with low density of defects and pinholes is essential. The usually used ZnO compact films are prepared by RF sputtering. RF sputtering method is a vacuum coating technology and its working processes are shown in Figure 2(d). A gas, usually argon, is purged into a vacuum chamber. Under a high frequency and high voltage electric field, it forms high energy ion flow. The ionized gas particles bombard a target and materials sputtered off the target deposited on a substrate and form a film made of the target material. The important parameters influence the product properties include composition and purity of target, work gas pressure, ratio of different work gases, RF power and so on. By optimizing these parameters, a high quality ZnO film with high transmittance and good electronic properties can be obtained.[81, 82] Because of the high energy coating process

and vacuum coating process, the adhesion between the film and substrate is steady and the quality of the product film is highly repeatable. As a result, RF sputtering method is an efficient method to fabricate ZnO ETM for PSCs application.

Tseng et al. studied the influence of ZnO film quality and RF sputtering parameters on solar cell performance.[83] In their research, compact ZnO films were fabricated by RF sputtering with different $O_2/(Ar+O_2)$ ratios (0, 10%, 20%, marked as Zn-Ar, Zn-10% and Zn-20% respectively), and planar heterojunction PSCs with structure of ITO/ZnO/$MAPbI_3$/spiro-OMeTAD were fabricated.

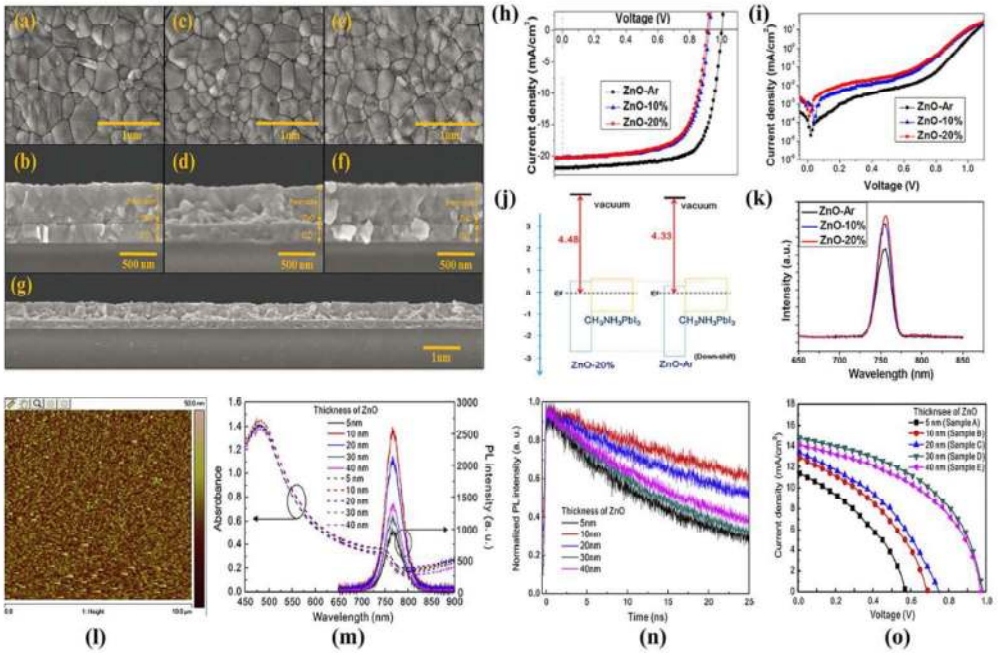

Figure 3. The surface morphologies and cross section images of perovskite films deposited on the ZnO-Ar film (a, b), ZnO-10% film (c, d) and ZnO-20% film (e, f). (g) Low magnification cross section view of a perovskite film deposited on the ZnO-20% film. (h) The J-V curves of PSCs based on ZnO-Ar, ZnO-10% and ZnO-20% films. (i) Dark current voltage characteristics of solar cells based on ZnO-Ar, ZnO-10% and ZnO-20% films. (j) The schematics of ZnO-Ar and ZnO-20% energy levels. (k) The

PL spectra of perovskite/ZnO-Ar, perovskite/ZnO-10%, and perovskite/ZnO-20% films. (l) Surface morphology of a thin layer of ZnO deposited on ITO glass. (m) UV-Vis absorption and PL spectra of the Perovskite/ZnO/ITO/glass structures with different ZnO layer thicknesses. (n) Time-resolved PL spectra of Perovskite/ZnO/ITO/glass films at λ = 768 nm under 405 nm excitation. (o) The J-V curves of perovskite solar cells based on ZnO films of different thicknesses.

The surface morphologies and cross section images of devices are shown in **Figure 3**(a-g). Different working gases have no obvious influence on the crystallinity and morphology of ZnO films deposited on ITO surfaces and likewise for perovskite films deposited on the ZnO surfaces. However, the performance of solar cells based on different ZnO films are quite different. The PCE of PSCs based on ZnO films deposited with different working gases are shown in Figure 3(h). As can be seen, solar cells consist of ZnO films prepared under pure argon show the best PCE of 15.9%, and the other solar cells based on ZnO films fabricated under O_2/Ar mixed gases show similar PCEs of about 12%.Considering that other components in both types of cells are the same, the increase in the PCE of the former can be attributed to the different fabrication processes of ZnO films. As well known, under ideal conditions, the stoichiometric ZnO is an insulator. However, due to the intrinsic defects existing in the lattice, ZnO materials generally show electrical conductivity. When there is stoichiometry deviation, in most cases, anion vacancies, interstitials, or oxygen defects are produced, which distorts the corresponding energy level and forms additional electron and donor levels. The donor levels are usually close to the conduction band edge. As a result, most ZnO

materials show the n-type character.[84] Therefore, pure Ar gas used during RF sputtering can lead higher oxygen deficiency concentration, which increases the conductivity of ZnO and lower the series resistance. This is confirmed by the dark current of solar cell which shown in Figure 3(i). As can be seen, solar cell based on ZnO-Ar shows the smallest dark current compared with solar cells based on ZnO-10% and ZnO-20%. In addition, when pure Ar gas is used during RF sputtering, the ZnO valence band will down shift, like shown in Figure 3(j). Lower conduction and valance band edge can enhance electron injection from perovskite to ZnO and block the hole more efficiently, which can be proved by the weaker photoluminescence (PL) intensity of perovskite film deposited on ZnO-Ar (shown in Figure 3(k)). Lower series resistance and high electron extraction efficiency lead a higher Jsc and Voc. On the other hand, the high charge extraction leads to smaller current hysteresis of solar cells based on the ZnO-Ar ETM than that of solar cells based on the ZnO ETM deposited with Ar/O_2 mixed working gases.[85]

Besides RF sputtering method, atomic layer deposition (ALD) technology is another common method to fabricate ZnO compact films. ALD is a technology derived from chemical vapor deposition (CVD), which has been widely used in semiconductor industry to produce high quality semiconductor films. As shown in Figure 2(e), one whole ALD deposition cycle is divided into four steps: 1) precursor A is pulse injected into a reaction chamber and form a single molecule film on substrate by chemical absorption; 2) the unreacted precursor is swept by an inert gas flow; 3) another precursor B is injected into the reaction chamber and then reacts with the precursor A

absorbed on the substrate, and a thin product film is formed; 4) the excess precursor and the by-products of the reaction are swept by the inert gas flow. Due to the limitation of chemical absorption, only a single molecule film will be formed every circle.[86] As a result, the whole process is accurately controlled and the coverage of product film is very high.[87, 88] Moreover, different from the RF sputtering method, the ALD coating process is more facile, which prevents the substrate from being damaged by high energy ions.[89]

Due to the facile process, high surface coverage and good electron transport ability of product film, ALD has been widely used to fabricate ultrathin and compact high quality ZnO ETM.[87, 90, 91] For ALD-ZnO films, the film thickness is an important factor affecting solar cell performance. Lee et al. systematically studied the effect of ZnO film thickness on PSCs performance.[92] In their research, they fabricated ZnO films with thicknesses ranging from 5 nm to 40 nm by ALD method and prepared PSCs with the structure of ITO/ZnO/$MAPbI_3$/Spiro-OMeTAD/MoO_3/Ag. As well known, the ITO usually used has rough surface, as shown in Figure 3(l), as a result, the 5 nm ZnO film can't fully cover the rough ITO surface, which forms a shunting path and decreases the solar cell performance. Figure 3(m,n) show the ultraviolet-visible (UV-Vis) absorption and PL spectra of perovskite/ZnO/ITO, as can be seen, with the thickness of ZnO film increase from 10 nm to 30 nm, the exciton dissociation at the interface between ZnO and perovskite is improved, which then improves the solar cell performance. Once the ZnO film thickness exceeds 30 nm, the series resistance of the ZnO film increases, which again decreases the photovoltaic performance. As a result, the best PCE of 7%

was achieved from the solar cell with 30 nm ZnO ETM. The J-V curves of PSCs based on the ZnO ETMs with different thicknesses are shown in Figure 3(o). In addition, according to research of Dong et al., the ALD ZnO film can promote the formation of $MAPbI_{3-X}Cl_x$ due to the reaction between ALD-ZnO and MACl.[93]

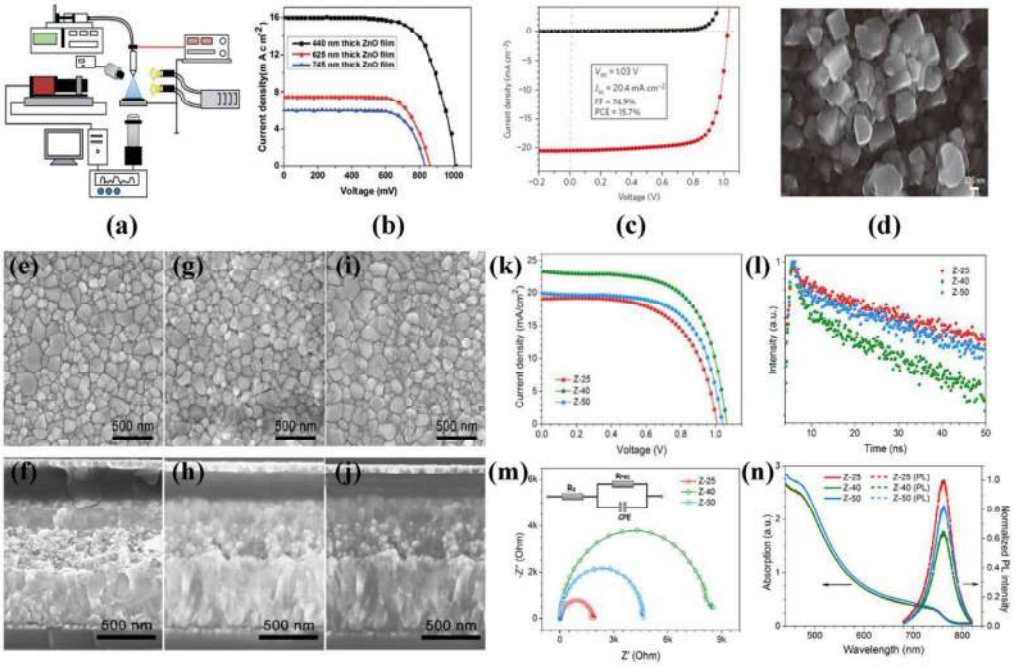

Figure 4. (a) The schematic illustration of an electrostatic spraying device. (b) The J-V curves of PSCs based on ZnO ETMs of different thicknesses. (c) The J-V curves of PSC with 25 nm ZnO nanoparticle film. (d) The surface morphology of perovskite on nanoparticle films. The surface morphology of perovskite films and cross section view of full PSC devices based on ZnO nanoparticles with size of 25nm (e, f), 40nm (g, h) and 50nm (i, j). (k) The J-V characteristics of PSCs based on ZnO mesoporous films with different sizes. (l) Time-resolved transient PL spectra of perovskite films on various ZnO mesoporous films. (m) The impedance spectra of PSCs based on ZnO ETMs of different particle sizes under 0.8 V applied bias in dark. The inset picture is

the equivalent circuit. (n) Absorption spectra and normalized steady-state PL spectra of perovskite films deposited on different ZnO films.

ZnO compact films for planar PSCs can be also obtained from electrostatic spraying method. The schematic illustration of electrostatic spraying device is shown in **Figure 4**(a). The general process of electrostatic spraying is that the precursor solution is sprayed and deposited onto a substrate under high voltage. The properties of ZnO films are tuned by changing substrate temperature, precursor solution flow rate (droplet size), substrate-to-nozzle distance, applied voltage and deposition time. Mahmood et al. reported planar PSCs based on ZnO films fabricated by the electrostatic spraying method.[94] In this research, they systematic studied the influence of spraying parameters on the morphology of ZnO thin films and fabricated PSCs based on the optimized ZnO film. According to their results, dense and uniform ZnO films can be obtained from large applied voltage, high substrate temperature, longer substrate-to-nozzle distance and suitable deposition time. Based on the mutual restriction between these parameters, they optimized the ZnO films and prepared PSCs based on ZnO films with different thicknesses furtherly. The J-V curves of these PSCs are shown in Figure 4(b). As can be seen, with the increase of ZnO film thickness from 440 nm to 745 nm, the PCE dropped from 10.8% to 3.4%. The drop of PCE mainly come from the increase of series resistance induced by the thicker ZnO ETM. Although the electrostatic spraying method has high deposition efficiency and good repeatability, ZnO film from electrostatic spraying has much more pinholes than ZnO fabricated by RF sputtering and ALD method.

3. PSCs based on ZnO nanoparticle ETMs

Apparently, due to the simple device structure and easy fabrication process, the planar PSCs based on compact ZnO ETM have achieved certain success. However, in many cases, the planar PSCs show more serious hysteresis than that of nonplanar PSCs. It is worth noting that this is not always true because fabrication methods and other layers also play an important role.[95-99] The so called hysteresis phenomenon is a change in shape of PSCs J-V curves under specific measurement conditions such as different voltage sweep rates, different sweep directions, or illumination history. Hysteresis lead to the underestimation of the real PSCs performance. To mitigate the hysteresis, the use of ETM with nanostructures, such as mesoporous structures, is a good solution, and mitigation of the hysteresis has been achieved for PSCs based on mesoporous TiO_2 ETM.[2,100] In addition, fast separation and extraction of carrier can efficiently reduce the recombination rate and improve the charge collection, which facilitates the performance of PSCs. The photo-induced carriers in PSCs are mostly separated by the electric field at the interface between perovskite and ZnO.[101] According the research of Kim et al., high density of states in the conduction band of perovskite will accumulate free carriers, which result in a longer extraction time.[102] Therefore, the carrier extraction efficiency can be significantly improved by the use of nanostructures due to its large specific surface area than planar structure. Furthermore, nanostructures can also work as scattering centers and increase the light harvesting in PSCs.

As a common nanomaterial, ZnO nanoparticles can be used directly to form porous

and dense films via facile solution method. The traditional methods of synthesizing ZnO nanoparticles are solution based synthesis methods. During the solution synthesis process, all precursors reacted in a solution, which means that the reaction process can be easily controlled. Among variety of solution based synthesis methods, sol-gel method is the most widely used method. Sol-gel process is a method of synthesizing materials at atmospheric pressure and low temperature.[103] To fabricate ZnO by sol-gel method, a common process is as follows. Firstly, a soluble Zn salt like $Zn(NO_3)_2$ or $Zn(CH_3COO)_2$ together with CH_3COOH as the catalyst and ethanolamine as the stabilizer are dissolved into an solvent such as 2-methoxyethanol to form a colloid solution. The colloid solution is spin coated or sprayed onto a substrate to form a ZnO film composed of ZnO nanoparticles. The diagram of this process is shown in Figure 2(f). The control of morphology, particle size and doping can be realized by changing the reaction parameters and precursor component, which have been widely reported.[104-108] Due to its simple and controllable synthesis process, ZnO nanoparticle film has been extensively studied and used as the ETM in traditional DSSCs and organic solar cells.[109-111] As for PSCs, ZnO nanoparticle films are first introduced by Liu et al.[3] They synthesized ZnO nanoparticles through a solution method and the general process is that: KOH and $Zn(CH_3COO)_2 \cdot 2H_2O$ were dissolved in methanol respectively, then KOH solution was added into $Zn(CH_3COO)_2 \cdot 2H_2O$ solution dropwise at 65 °C over 15 min. The mixed solution was stirred for 2.5 h at 65 °C. After the reaction, the precipitate was washed twice by methanol and redispersed in a mixed solvent containing n-butanol, methanol and chloroform. With the ZnO nanoparticle dispersion, ZnO nanoparticle

films with thickness range from 0 nm to 70 nm were deposited by spin coating. Subsequently, they fabricated planar heterojunction PSCs with structure of ITO/ZnO/$MAPbI_3$/spiro-OMeTAD/Ag. With the increase of ZnO film thickness from 0 nm to 25 nm, the PCE of PSCs improved from 2.4% to 14.4% and the PCE decrease to 12.9% once the ZnO film thickness continues to increase to 70 nm. This result consisted with the earlier reports on the effect of ZnO thickness mentioned above. To ensure the reproducibility of the results, a large number of PSCs based on 25 nm ZnO films were prepared, and a highest PCE of 15.7% was obtained, and the J-V curve of best performing PSC is shown in Figure 4(c).

In addition, they found that the grain size of perovskite on planar ZnO film was larger than that on mesoporous TiO_2 film, as shown in Figure 4(d). This is because that when deposited on mesoporous film, the perovskite infiltrate into the pores and the growth of perovskite grain will be restricted by the pore size. And when planar ZnO films were used as ETM, without the limitation of mesoporous structure, larger perovskite crystallite size was obtained. The larger grain size can reduce the grain boundaries in perovskite films, which reduce recombination and series resistance. Meanwhile, the crystallites also act as efficient light scattering centers, which increase optical path and hence absorption. Both of these two factors will increase the Jsc of PSCs.

Apart from the film thickness, the particle size also affects the solar cell performance. Zhang et al. systematically studied the ZnO nanoparticle size effect on solar cell performance.[112] In their research, they synthesized a series of ZnO

nanoparticles with different sizes (25 nm, 40 nm, 50 nm) and fabricated PSCs based on the mesoporous ZnO ETMs (FTO/ZnO compact film/ZnO mesoporous film/perovskite/spiro-OMeTAD/Au). The surface morphology of perovskite films and cross section view of PSCs based on ZnO nanoparticles of different sizes are shown in Figure 4(e-j). As can be seen, the influence of particle size on solar cell performance mainly comes from the pore filling effect of perovskite into ZnO mesoporous films. Poor filling of small particle (25 nm) films leads to serious recombination while large particle films (50 nm) with high perovskite filling and a low contact area reduces the charge injection efficiency from the perovskite absorber to the ZnO ETM layers. This is consisted with the PL spectra, EIS test and UV-Vis absorption spectra results shown in Figure 4(l-n). As a result, the best PCE of 15.92% was obtained from the film with moderate particle size (40 nm), and for smaller and larger particle sizes, PCEs of 11.86% and 13.20% were obtained, respectively, the J-V curves are shown in Figure 4(k).

Besides the widely used n-i-p solar cell structure mentioned above, the p-i-n solar cell structure is also widely researched. When the p-i-n structure is used, the ETM will be deposited on the top of the perovskite film rather than between perovskite and transparent electrode. Compared with the organic ETM, the inorganic ZnO ETM has strong resistance to oxygen and vapor in the air. As a result, ETMs made of ZnO nanoparticle film can improve the stability of PSCs to some extent. You et al. reported related research in 2016.[41] In their research, they fabricated PSCs with structure of ITO/NiO_x/Perovskite/ZnO/Al. Inorganic NiO_x and ZnO were respectively used as the HTM and ETM to replace the conventionally used PEDOT:PSS and PCBM. The NiO_x

layer was prepared from a Ni precursor solution composed of ethylene glycol and $Ni(NO_3)_2 \cdot 6H_2O$. The precursor solution was spin coated on ITO and annealed to form NiO_x film. The ZnO film was prepared by similar method reported by Liu et al.,[3] but in order to prevent perovskite film from being damaged, ZnO nanoparticle was dispersed in chlorobenzene instead of methanol mixed solution. The solar cell with metal oxide charge transport materials gained a PCE of 16.1%, and more importantly, compared with solar cells using organic HTMs and ETMs, the stability of all metal oxide solar cells was significantly improved: the PSCs with NiO_x and ZnO maintained 90% performance over 60 days of testing in ambient air at room temperature and with 30-50% humidity, however the performance of PSCs based on PEDOT:PSS and PCBM dropped dramatically.

Since the PCE and long term stability of PSCs have made great progress, the extensive production of PSCs has become another area worth studying. While the most widely used method to fabricate PSCs is spin coating, which is not suitable for mass production, hence, the effective and low cost roll-to-roll method is a good alternative. However, roll-to-roll method can be carried out only with the process temperature within 100 ºC - 150 ºC.[113] For widely used TiO_2 ETM, both planar and mesoporous films need high temperature (450 ºC) annealing. Although low temperature TiO_2 fabrication processes have been reported,[114] the performance of PSCs based on low temperature TiO_2 is still not comparable with that based on high temperature TiO_2. As for PEDOT:PSS and PCBM, the process temperature is no longer a limit, but the low stability of PSCs can't be ignored.[41] As a result, high quality ZnO nanoparticle films

with low process temperature are good choice for now.

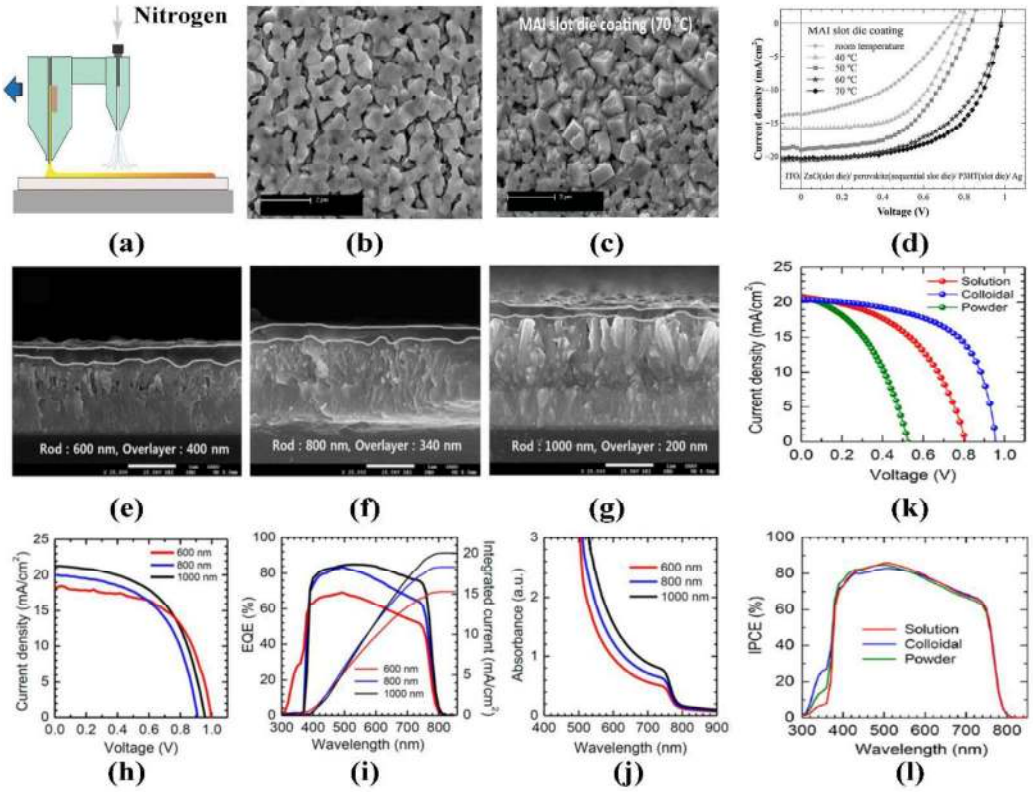

Figure 5. (a) A diagram of the slot die coating system. (b) The surface morphology of PbI_2 film obtained from N_2 quenching slot die coating. (c) The surface morphology of perovskite film obtained from hot slot die coating. (d) The evolution of J-V characteristics with the different hot coating temperatures. The cross section of PSCs based on ZnO nanorods of (e) 400 nm, (f) 800 nm and (g) 1000 nm. (h) J-V curves and (i) EQE spectra together with EQE data-based integrated current density for the PSCs based on ZnO nanorods of different lengths. (j) Absorption spectra of the perovskite films on ZnO nanorods of different lengths. J-V curves (k) and IPCE spectra (l) of solar cells based on ZnO nanorods grown from different seed layers.

Hwang et al. reported the fabrication of fully slot-die coated PSCs.[115] In this research, they fabricated fully printable PSCs, with exception of metal electrodes,

which were evaporated, by the slot-die coating method with a home-made 3D printer. A schematic diagram of the printer is shown in **Figure** 5(a). In this 3D printer system, the space position and motion of nozzle can be controlled by predefined programs. Temperature of the substrate and nozzle are also controlled. By using this equipment, the ZnO ETM, doped poly(3-hexylthiophene) (P3HT) HTM and $MAPbI_3$ film were successfully fabricated. To improve the crystallization of the $MAPbI_3$ film, the N_2 quenching and hot slot-die were used; the improved quality of the PbI_2 film promotes the reaction conversion reaction of PbI_2 to perovskite. As shown in Figure 5(b), N_2 quenching is used to quickly dry the PbI_2 film by a N_2 flow, which leads to a porous PbI_2 film and makes MAI easy to permeate. The hot slot die process involves heating the substrate to a set temperature to facilitate the reaction and the temperature of substrate is important to the film quality and solar cell performance. The morphology of a perovskite film obtained under a substrate temperature of 70 ^oC is shown in Figure 5(c) and the PCE of solar cells based on perovskite films obtained from different substrate temperatures are shown in Figure 5(d). The best PCE of 11.96% was obtained from devices fabricated by slot-die coating when substrate temperature is 70 ^oC in ambient. These results verify the possibility of the roll to roll method in low cost PSCs production.

As for flexible PSCs, the mechanical strength of cells is another problem worth considering. To improve the mechanical strength of flexible devices and simplify the structure, Zhou et al. report a hole-conductor-free and metal-electrode-free solar cell structure, which is ZnO/perovskite/carbon solar cell structure.[116] By using this unique

structure, they gained a PCE of 8.73% on a grid substrate and 4.29% on a flexible substrate. Their devices can maintain 80% of its initial efficiency even after 1000 times of bending.

4. PSCs with ZnO nanorods ETMs

ZnO nanoparticles have been proved to be an effective ETM for PSCs, but in ZnO films made of nanoparticles, electrons have to travel across many particles before they reach the electrodes. Electron transport becomes less efficient when the photocurrent increases because of the serious surface recombination. This limits the further increase of solar cell efficiency. As a result, in order to reduce the severe recombination, one dimension ZnO nanostructures were used to replace nanoparticle films. Unlike nanoparticles, the one-dimensional ZnO nanostructures usually is single crystal and provide a direct pathway for electron transport.[62] Among various one-dimensional structures, ZnO nanorods is the most widely used material for solar cells.

A traditional method of fabricating ZnO nanorods is hydrothermal method. The hydrothermal method is a synthesis method of crystal materials in hot water or organic solvents under high temperature. The basic principle of hydrothermal method for ZnO synthesis is as follows. A Zn salt and alkali, e.g. KOH or hexamethylenetetramine, are dissolved into the solvent. The Zn^{2+} and OH^- in the solution react with each other to form $Zn(OH)_2$ precipitates. As the reaction proceeds, the temperature and pressure increases, the pH of the solution increases gradually, and the concentration of Zn^{2+} decreases, which lead to decomposition and dehydration of $Zn(OH)_2$ precipitates. Finally, the $Zn(OH)_2$ precipitates convert into ZnO.[117] Like other solution based

synthesis methods, the morphology and doping of ZnO nanorods can be realized by tuning the composition and concentration of precursor, reaction temperature and time.

ZnO nanorods were introduced into PSCs by Bi et al. in 2013.[118] They fabricated the PSCs on the basis of experience and knowledge accumulated from traditional DSSCs. In their research, by using $MAPbI_3$ as the sensitizer and combining solid spiro-OMeTAD HTM and ZnO nanorods ETM, they prepared PSCs with the structure of Au/spiro-MeOTAD/$MAPbI_3$/nanorods/seed layer/FTO. The ZnO nanorods were synthesized from the hydrothermal method. Compact ZnO film prepared from ZnO colloids were used as a seed layer for hydrothermal as well as an hole block layer. The obtained ZnO nanorods were vertically aligned on the substrate. The $MAPbI_3$ sensitizer was made from a precursor solution (PbI_2:CH_3NH_3I=1:1, molar ratio, 40 wt% in γ-Butyrolactone (GBL)) by spin coating. After spin coating, the $MAPbI_3$ will penetrate into the space between the nanorods without affecting ZnO nanorods. They studied the relation between the nanorods length and cell performance. It was found that the length of nanorods plays a key role in cell efficiency. To certain extent, with increasing the ZnO nanorods length, the Jsc, FF, Voc and PCE of solar cells increase but the Voc may decrease. This is mainly because the length of ZnO nanorods determines the electron transport time and lifetime, which will directly affect the performance of solar cells. Although the best PCE they gained is only about 5.0%, the work opens a new direction for the ZnO ETM based PSCs.

Similar study has been reported by Son et al.[119] In their research, they fabricated PSCs with the same device structure. Because the morphology and quality of perovskite

materials fabricated by the initial one step coating process can't be tightly controlled. Perovskite can't always completely fill and cover the space between the nanorods, and the spiro-OMeTAD can permeate into these unfilled holes and contact with ZnO nanorods, which will form shunt path and deteriorate the performance of solar cells. Therefore, they used a two-step coating method to replace the one step method used by Bi et al.[118] The cross section of PSCs based on ZnO nanorods of different lengths were shown in Figure 5(e, f, g). As can be seen, the two-step coating method produced a fully filled perovskite film covered all ZnO nanorods of different lengths without voids and formed an overlayer on the nanorods surface. Additionally, the two step coating procedure optimizes the cuboid size of $MAPbI_3$ and then decreases the series resistance of the PSC, which is favored by solar cells.[120] As a result, combing the two step coating method with the optimized nanorods length, a best PCE of 11.13% was obtained.[119]

Further research on the relation between the nanorods length and solar cell performance was carried out either. The J-V curves, external quantum efficiency (EQE) spectra together with EQE data-based integrated current density for the PSCs based on ZnO nanorods of different lengths are shown in Figure 5(h) and (i). As can be seen, with the increase of ZnO nanorods length, the PCE, Jsc and EQE of solar cell increase too, while the Voc decreased. The increase of PCE and Jsc are because longer nanorods increase the charge extraction efficiency and the nanorods also act as scattering centers to increase the light absorption, which is confirmed by the UV-Vis absorption spectra of the perovskite films on ZnO nanorods of different lengths shown in Figure 5(j). The decrease of Voc can be attributed to larger interfacial area induced by increasing

nanorods length, which increased the recombination at the same time.

Besides the length of nanorods, the seed layer plays an important role in the ZnO nanorods growth and photovoltaic performance of the solar cells.[121-123] The so called seed layer is usually a compact ZnO film, which is usually fabricated by solution processes. Generally, there are three kinds of precursor solutions can be used to fabricate ZnO seed layers. The precursor solutions can be zinc salt solution, ZnO colloids or ZnO nanoparticle solution. Son and his colleagues systematically deposited three different ZnO seed layers based on each precursor solution and studied the influence of on ZnO nanorods growth and photovoltaic performance of PSCs.[124] According to their results, the seed layer can affect the properties of ZnO nanorods. Seed layer produced from the colloid solution can fully cover the substrate, and however, the seed layer made from the zinc salt solution or ZnO nanoparticle solution does not provide a full coverage. The poor coverage of ZnO films tends to form shut paths. ZnO nanorods grow on a colloid seed layer showed not only a good coverage but also enhanced transmittance over the range of visible wavelengths. The shunts caused by the poor coverage decrease the Voc and photocurrent density, as shown in Figure 5(k, l). In addition, recombination at the perovskite/ZnO interface was suppressed for the cell using the seed layer prepared by the colloid solution. This work directly proved the important role of the seed layers for the ZnO nanorods based PSCs.

On the other hand, considering the unique structure and morphology of ZnO nanorods, it's difficult to fabricate high quality perovskite films on nanorods surfaces. As a result, preparation of high quality perovskite film with good surface morphology,

grain size and coverage are another area worthy of study.

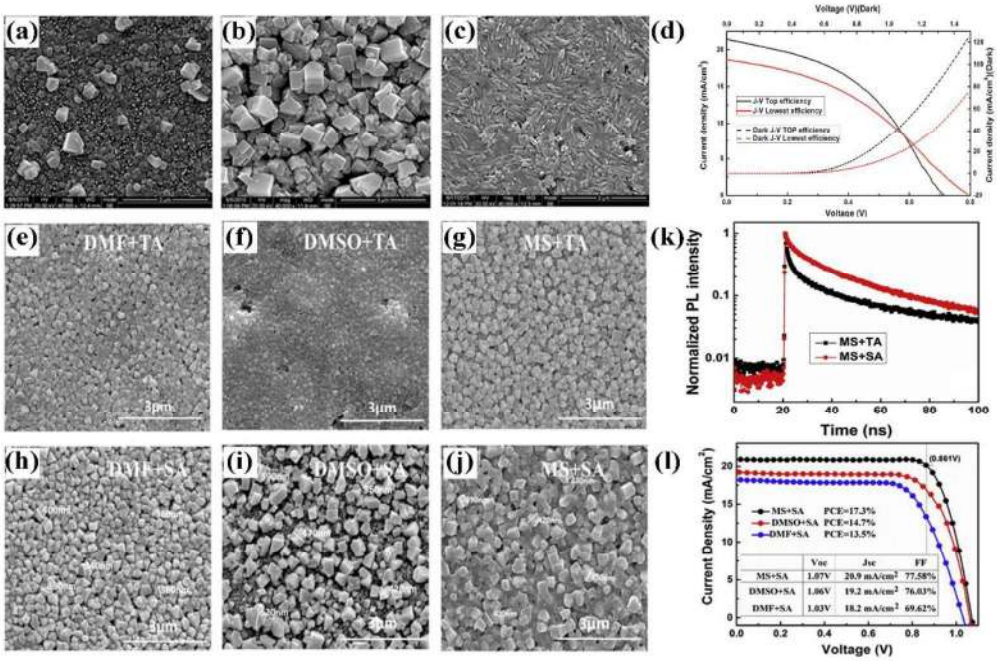

Figure 6. The surface morphology of perovskite films fabricated from the traditional sequential method with pure DMF solvent on (a) 3 μm ZnO nanorods and (b) 1 μm ZnO nanorods. (c) The morphology of a perovskite film fabricated on 1μm ZnO nanorods using the DMF/DMSO mixed solution as solvent. (d) The J-V curves of the best and worst performed PSCs based on the modified sequential method. The perovskite films fabricated from the sequential method with (e) DMF, (f) DMSO and (g) DMF/DMSO mixed solution as solvent under thermal annealing (TA) and perovskite films prepared from (h) DMF, (i) DMSO and (j) DMF/DMSO mixed solution under solvent annealing (SA). (k) Time-resolved PL spectra of perovskite films fabricated from the mixed solvents along with solvent annealing. (l) J-V curves and photovoltaic parameters of PSCs fabricated from different methods.

To solve this problem, our group has developed a solvent engineering method to

fabricate high quality and uniform perovskite films.[125] In our research, PSCs based on ZnO nanorods of different lengths were fabricated and a N,N-Dimethylformamide/Dimethyl sulfoxide (DMF/DMSO) mixed solvent was used as an alternative to the usually used DMF to fabricate perovskite precursor solution. As a control, perovskite films prepared from pure DMF solvent were deposited on ZnO nanorods with length of 3 μm and 1 μm, and the surface morphologies of perovskite films are shown in **Figure** 6(a) and (b). It is obviously that the perovskite films cannot fully cover the surface of ZnO nanorods, which is detrimental to the device. The morphology of perovskite film prepared by DMF/DMSO mixed solution was shown in Figure 6(c). As can be seen, the existence of DMSO results in a uniform and high quality film with full coverage of the ZnO nanorods surface. In the mixed solution, the DMF simply served as a solvent while the DMSO react with PbI_2 to form PbI_2(DMSO) complex. When PbI_2(DMSO) contacts with MAI, the DMSO is replaced by MAI easily because of its higher affinity of towards PbI_2 compared to DMSO. As a result, DMSO in the solvent will retard the crystallization of perovskite and lead to a high property film.[35, 126] The PSC based on mixed solvents gained the best PCE of 6.63% (Figure 6(d)). The unexpected low efficiency may attribute to the poor crystallization of the $MAPbI_3$ layer, and the supposition was proved by the low film quality as shown in the SEM images and XRD patterns.

In order to further improve the quality of crystallization, we developed a solvent annealing method on basis of the solvent engineering work.[125, 127] In this study, ZnO nanorods were fabricated by hydrothermal method either. An ultrathin Al_2O_3 film was

deposited on the surface of ZnO nanorods by ALD method. The perovskite film was prepared by a two-step spin coating method. PbI_2 and MAI precursor solution were prepared by a mixed solvent DMF/DMSO (MS) and isopropanol respectively. To fabricate perovskite film, ZnO nanorods were first infiltrated with PbI_2 by spin coating and dried at 70 ºC. After cooling to room temperature, the films were immersed in the MAI solution and then dried. As a control, pure DMF and DMSO were also used to fabricate perovskite film. The SEM pictures of perovskite films fabricated from different solvents were shown in Figure 6(e)-(g). As shown in the figures, the perovskite film prepared by pure DMF has larger grain size than films based on pure DMSO, while both films has many pinhole. However, for perovskite film prepared by mixed solution, a uniform and compact film with less pinholes and smaller grain size was obtained.

The different morphology can be attributed the different properties of different solvents as mentioned above. In addition, during this process, we found that the mixed solvent DMF/DMSO can lead to a mesoporous PbI_2 film, and the mesoporous structure can provide a larger contact area between PbI_2 film and MAI solution. The mesoporous structure promotes the formation of $MAPbI_3$ when the PbI_2 film was immersed in MAI solution. Although all the obtained $MAPbI_3$ films have large grains, there are still some small pinholes existed in the film, and the pinholes are the main reason for poor photovoltaic performance. To solve this problem, a solvent annealing process is introduced via annealing the $MAPbI_3$ film in the ethanol vapor atmosphere. The surface morphologies of perovskite films fabricated from thermal annealing (TA) and solvent annealing (MA) methods are shown in Figure 6(h)-(j). As can be seen, after solvent

annealing, the grain size of perovskite films obtained from three different solvents both increased. The pinholes in perovskite films fabricated from pure DMF and DMSO did not disappear. While the perovskite films prepared by mixed solvent have no pinholes in sight. This is because in ethanol atmosphere, the MAI is dissolved and continue to react with PbI_2. As for perovskite films based on pure DMF and DMSO, pinholes in the film will be intensified by annealing the solvent annealing. As a result, the grain size and compactness of the $MAPbI_3$ film are improved after solvent annealing, which is consisted with the film morphology. Compact films with larger grain sizes decrease the number of grain boundaries and density of defects, which are favorable to improve the photovoltaic performance.[128, 129] In addition, ZnO nanorods passivated with a thin Al_2O_3 layer improve charge collection in the PSCs, which is confirmed by the transient PL spectra of different perovskite films and J-V curves shown in Figure 6(k) and (l). As a result, the combination of the three methods boosts the PCE of PSCs to 17.3%, which is the highest efficiency for ZnO nanorods based PSCs.

5. PSCs based on other ZnO nanostructures

5.1 ZnO nanowalls

ZnO nanowalls is a kind of sponge-like ZnO nanostructures with a large 2D framework and surface area, and like ZnO nanorods, this structure offers a large contact area and direct electron transport path. As a result, ZnO nanowalls have been widely used in energy storage devices and biosensors because of its larger surface area than nanorods. Tang et al. synthesized ZnO nanowalls by a low temperature chemical bath method and fabricated PSCs based the ZnO nanowall ETM.[130] In this research, Al was

first deposited on ITO surface as template before the growth of ZnO nanowalls. Equimolar $Zn(CH_3COO)_2 \cdot 2H_2O$ and hexamethylenetetramine were dissolved in water to fabricate precursor solution, and then ZnO nanowalls were grown on the substrate by chemical bath process. After the deposition of perovskite, spiro-OMeTAD HTM and Ag electrode, PSCs with structure of ITO/ZnO nanowalls/perovskite/HTM/Ag were obtained. A planar PSC based on ZnO compact film was prepared as a control device. The compact ZnO film for planar PSC was prepared by spin coating the precursor solution composed of $Zn(CH_3COO)_2 \cdot 2H_2O$ and monoethanolamine on the ITO substrate.

The best performance PSC based on ZnO nanowalls produced a J_{SC} of 18.9 mA/cm^2, Voc of 1.0 V, FF of 72.1% and PCE of 13.6%. While, the control device shows a Jsc of 18.6 mA/cm^2, Voc of 0.98 V, FF of 62% and PCE of 11.3%. The introduction of ZnO nanowalls leads to an obvious improvement in the FF and PCE of the PSCs. This is because ZnO nanowalls offer much larger contact area between ZnO and perovskite material than the planar ZnO film, which improves the electron collection and transportation efficiency at perovskite/ZnO nanowalls interface. Moreover, because of the alkaline behavior of the ZnO surface, the perovskite will be decomposed by ZnO and lead to formation of PbI_2 on the interface of perovskite/ZnO, and the presence of PbI_2 can suppress the surface recombination and improve the FF.[36]

However, PbI_2 from perovskite decomposition obviously cannot be controlled. In addition, PbI_2 was not discovered in perovskite on compact ZnO film (control device) according to their research. This indicates that surface of ZnO nanowalls is more

reactive than compact ZnO film, which means that perovskite on ZnO nanowalls is more unstable. This is harmful to the reproducibility and performance of PSCs.

5.2 ZnO nanowires

ZnO nanowires are another widely used one-dimensional structures, which is similar to nanorods. Benefit from its high aspect ratio and good crystallization, ZnO nanowires are efficient to provide large surface area and improve the electron transport. As a result, ZnO nanowires have been widely used and studied in DSSCs.[62, 131] But researches about PSCs based on ZnO nanowires were deficient.

Hu et al. reported a flexible PSC based on a single ZnO nanowire.[132] In their research, the ZnO nanowires were fabricate via a vapor-liquid-solid (VLS) process developed by Zhu et al.[133] After the growth of ZnO nanowires, a single nanowire was transferred onto a polystyrene (PS) substrate and fixed by silver paste electrode. $MAPbI_3$ and spiro-OMeTAD are subsequently deposited on one end of the ZnO wire to form the solar cell. The PSCs based on single ZnO nanowire show a PCE of 0.0338%, the extremely low PCE is mainly due to the small effective illumination area of the PSC.

Moreover, they found that the piezo-photo-tronic effect of ZnO nanowires can improve the performance of PSCs based on ZnO nanowires obviously. The PCE increased from 0.0338% under 0 strain to 0.139% under 0.47% strain. This is because that when an external force is applied, the piezo-phototronic effect leads to a shift of the conduction band and suppresses the interface recombination, which result in the higher Voc and Jsc. This method indicates that ZnO nanowires are efficient ETM for PSCs, while confined to the micron scale effective illumination area, the PCE of PSCs

is extremely low. However, the small size of flexible PSCs based on single ZnO nanowires may have potential applications in integrated devices. Moreover, the studies on performance enhancement due to piezoelectric effects provide a new approach to improve the properties of PSCs.

5.3 ZnO quantum dots

Compared with other ZnO nanostructures, ZnO QDs show many unique properties. Firstly, due to its small size, the quasi continuous energy levels of bulk materials are replaced by the separated electronic energy levels and the band gap will become larger. The increased band gap are mainly caused by the negative shift of the conduction band and the positive shift of the valence band, which will improve the electron injection efficiency. Secondly, after absorbing a photon, QDs can produce more than one exciton, which is beneficial to improve the performance of solar cells.[134-136]

Ameen et al. fabricated a flexible planar PSC based on ZnO quantum dots for the first time.[137] In this research, ZnO QDs were prepared by solution process method. The $Zn(CH_3COO)_2 \cdot 2H_2O$ and $(CH_3)_4NOH \cdot 5H_2O$ were dissolved in ethanol respectively to form precursor solution. Subsequently, the $(CH_3)_4NOH \cdot 5H_2O$ solution was added dropwise into $Zn(CH_3COO)_2 \cdot 2H_2O$ solution. After two hours of reaction, the obtained solution was centrifuged and dispersed for several times, and the finally obtained ZnO QDs were dispersed in ethanol. To fabricate ZnO QDs based PSCs, the graphene film, ZnO QDs film and perovskite film were deposited on ITO-PET (Polyethylene terephthalate) substrate sequentially. During the fabrication process, the ITO-PET substrate and ZnO QDs film was treated by O_2 plasma and atmospheric

plasma jet (APjet) before the next step deposition. After the deposition of spiro-OMeTAD HTM and Ag electrode, a PSC with structure of ITO-PET/Graphene/ZnO-QDs(APjet treatment)/$MAPbI_3$/spiro-MeOTAD/Ag.

With the graphene blocking layer and the APjet treatment, a best PCE of 9.73% with J_{SC} of 16.8 mA/cm^2, V_{OC} of 0.935 V, and FF of 62%. To determine the role of ZnO QDs and APjet treatment, control devices based on ITO-PET/Graphene and ITO-PET/Graphene/ZnO QDs films (without APjet treatment) were fabricated either. And the PCE of PSC based on ITO-PET/Graphene was 2.89% with J_{SC} of 12.03 mA/cm^2, V_{OC} of 0.840 V, and FF of 29%. As for PSC based on ITO-PET/Graphene/ZnO QDs(without APjet treatment), a PCE of 5.28% with J_{SC} of 14.97 mA/cm^2, V_{OC} of 0.830 V, and FF of 43% were obtained. Obviously, the introduction of ZnO QDs and APjet treatment obviously improved the performance of PSC. The main reason is that the ZnO QDs film can provide a larger contact area than compact graphene film and the APjet treatment improved the porosity and surface area of ZnO QDs film, which significantly increased the light scattering and the interaction between the $MAPbI_3$ film and ZnO-QDs interfaces, leading to an improved Jsc. In addition, the PSC based on ZnO QDs with APjet treatment shows a higher electron transport and charge collection, which result in a high Jsc and Voc. As a result, the ZnO QDs and APjet treatment are essential for high performance PSC.

However, large specific surface area and large amount of surface atoms of ZnO QDs lead to the lack of coordination of surface atoms and increase of unsaturated bonds. As a result, these surface atoms are high activity and extremely unstable, which are

very easy to combine with other atoms. Hence, the ZnO QDs are unstable, which will restrict its extensive application.

Based on ZnO ETM with various morphologies, the performance of PSCs have made great progress. Moreover, its application has been expanded to flexible devices and roll to roll method without the limitation of high temperature process. However, the performance of PSCs based on ZnO ETM is still not comparable to that of PSCs based on TiO_2 ETM. As a result, the following presents the challenges for PSCs based on ZnO ETM and solutions to the problems.

6. The modification of ZnO ETMs for efficient PSCs

Although the performance of ZnO ETM based PSCs has made great progress, the PCE of ZnO ETM based devices are still inferior to those solar cells based on TiO_2 ETM. The first problem restricts the further development of ZnO ETM based solar cells is the serious surface recombination. As well known, perovskite materials have high carrier mobility and reduced internal recombination, therefore the surface recombination plays an important role determining the performance of PSCs.

The recombination firstly come from the intrinsic defects of ZnO. Similar to other semiconductor materials, point defects affect the electrical and optical properties of ZnO. There are six kinds of point defects in ZnO, which are Zn vacancies (V_{Zn}), oxygen vacancies (V_O), zinc interstitial (Zn_i), oxygen interstitials (O_i), zinc antisites (Zn_O) and oxygen antisites (O_{Zn}). Among them, V_O, Zn_i and Zn_O are donor defects and V_{Zn}, O_i and O_{Zn} are acceptor defects.[84] Besides the defect level position, the effect of defects on ZnO properties also depends on the defect concentration. The concentration of

defects is not an eternally fixed constant because of the formation energy of defects will change under different conditions. The relationship between formation energy and concentration of defects is shown **Equation 1**:[138]

$$C=N_{sites}exp\left(-\frac{E^f}{k_BT}\right) \quad (1)$$

Where N_{sites} is the number of sites (including different configurations) per unit volume the defect can be incorporated on, E^f is the formation energy of defects, k_B is the Boltzmann constant and T is temperature. The formula reveals a negative exponential relation between defect concentration C and formation energy E^f, which means that a higher formation energy will lead to a lower equilibrium defects concentration. According theoretical calculation and experimental results of Kohan et al. and Oba et al., in N type ZnO, V_O shows the lowest formation energy of 0.02 eV and has the largest concentration. Zn_i also has relatively low formation energy and high concentration. Because of the high formation energy of V_{Zn}, O_i and O_{Zn}, the concentrations of these acceptor defects are very low. As a result, the V_O and Zn_i play key roles in ZnO.[139,140] Besides these point defects, when perovskite materials deposited on ZnO surface, the large lattice mismatch at ZnO/perovskite interface can be observed, which have been verified by the computational analysis.[141]

The surface state of ZnO film is another source of recombination. At the surface, the crystal structure of ZnO is abruptly interrupted, which forms a large amount of dangling bonds and defects. This problem is particularly obvious in ZnO nanostructures because of the significant increased specific surface area, for example, 30% of the atomic bonds in ZnO nanoparticles are dangling bonds.[142] In addition, once exposed

to the air, oxygen and H_2O in the air will be absorbed by ZnO surface, which will also form a recombination center on the surface. In addition, the adsorbate and ZnO surface formed a structure similar to a Schottky barrier due to the charge transfer between adsorbates and the ZnO surface, which changes the carrier concentration within the surface space charge region. Some adsorbates such as OH molecules lead to band bending and charge accumulation near the ZnO surface, which will change the surface conductivity.[143,144]

Besides the above-mentioned, the fabrication process, especially for the solution process, will introduce new defects. ZnO materials prepared by chemical methods, such as the hydrothermal method, chemical bath deposition and sol-gel method, are not likely pure crystals, and organic species and chemicals from the precursor solutions used in the fabrication process will be left or absorbed on ZnO surface.[145,146]

These defects mentioned above can reduce the performance of PSCs by providing extra recombination pathways so that the incident light cannot be convert to electricity. The defects induce deep energy levels in ZnO band gap and give rise to a high density of recombination centers, which will reduce the lifetime of photo generated carrier and the quantum efficiency of PSCs. The result of such a process is the increased inner resistance and large dark current of PSCs, and the decreased photocurrent. Furthermore, the surface conduction layer induced by the surface absorption of ZnO can affect the carrier extraction at the perovskite/ZnO interface, which will also decrease the photocurrent and open circuit voltage of PSCs. Due to serious impacts of these defects, the characterization of defects is necessary. The common method to investigate defects

include Photoluminescence (PL),[36,147,148] Time-Resolved Photoluminescence (TRPL),[149] Electrochemical Impedance Spectroscopy (EIS) and X-ray photoelectron spectroscopy (XPS).[61,150] Since the systematic studies about these methods have been widely reported, readers can refer to relevant information in the references.

Besides the recombination, another serious problem is the poor stability of ZnO based PSCs. Perovskite materials are known to sensitive to water and oxygen in the air but thermally stable under some conditions.[151] However, according to research of other authors and our group, perovskite deposited on ZnO is easily to decompose during thermal treatment. Such phenomenon is not found between TiO_2 and $MAPbI_3$. This is mainly because the different surface properties of ZnO materials. The surface of TiO_2 showed slightly acidic while the surface of ZnO exhibits basic behavior. Once perovskite contacts with ZnO, deprotonation reaction against methylammonium cation happens, which is the root of instability, and this assumption has been proved by theoretical calculations.[141] Another important reason for instability is chemical residues from fabrication processes. ZnO materials especially nanomaterials used for PSCs are usually synthesized by chemical solution methods, therefore, the chemicals in the solution are unavoidably left on the ZnO surface. According to the research of Yang et al. and Cheng et al.,[141, 152] the hydroxyl groups and residual acetate from the growth solution exacerbate the decomposition of perovskite. This is because the ZnO materials synthesized by the solution process are not completely oxidized, and the surface of the obtained ZnO nanomaterials are covered with chemisorbed oxygen species like hydroxide, which could break the ionic interaction between $CH_3NH_3^+$ and

PbI_3^- and destroy the crystal structure of the $MAPbI_3$ sequentially. This process can be explained by the reaction formula as follows:

$$OH^- + CH_3NH_3I \rightarrow CH_3NH_3OH + I^-$$

$$CH_3NH_3OH \rightarrow CH_3NH_2\uparrow + H_2O \text{ (heat)}$$

Obviously, the reaction between hydroxide on the CH_3NH_3I can directly decompose the perovskite under annealing. Along with the ZnO introduced deterioration, the decomposition process of ZnO/perovskite system accelerates at elevated temperatures.

Furthermore, according to our research, the performance of PSCs based on ZnO ETM will gradually degraded under full spectrum AM 1.5G illuminations for extended exposure time. This is because that ZnO shows high photocatalysis activity under the illumination of ultraviolet (UV) light with wavelength less than 400 nm and the simulated sunlight contains about 4.6 mW/cm^2 of UV light less than 400 nm in the spectrum. As a result, under the excitation of UV light, ZnO will decompose the perovskite materials atop its surface. More seriously, surface hydroxyl groups and chemical residues on ZnO surface will induce photochemical reactions and further accelerate the decomposition of perovskite.[153]

In order to improve the performance of ZnO based PSCs, the high recombination loss and chemical instability must be solved. According to the Shockley Read Hall (SRH) theory, there are two technical means to reduce the surface recombination: 1) reduce the density of surface states; 2) reduce the concentration of free electrons and holes at the surface. The surface state concentration can be reduced by depositing or

growing a suitable material with low surface recombination velocity on the surface and the concentration of free carriers can be reduced by doping, which are the two most commonly used methods.[154]

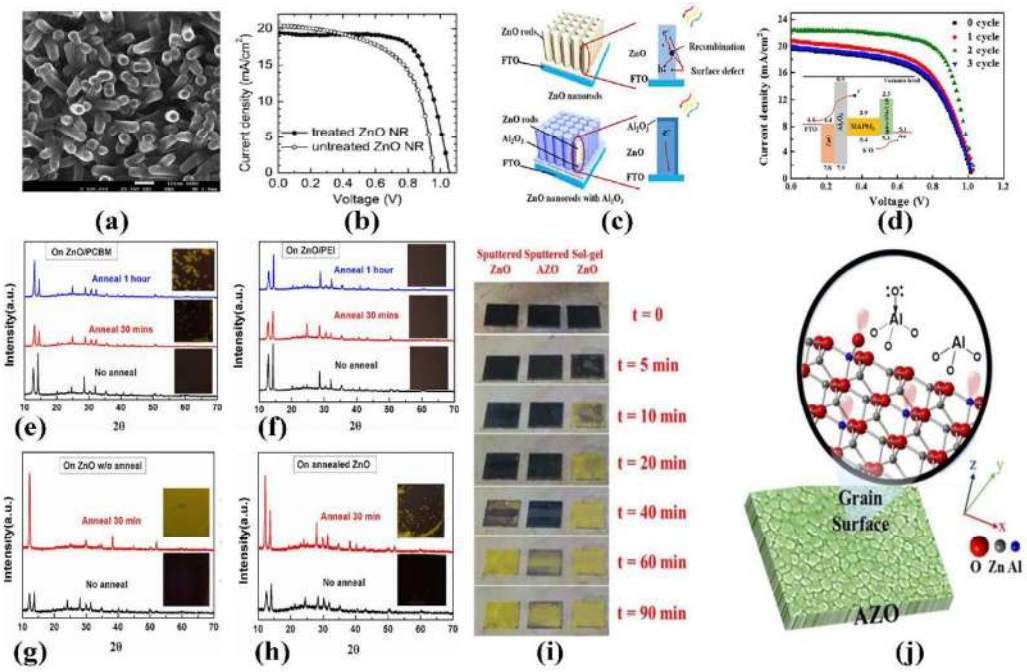

Figure 7. (a) The surface morphology of TiO_2 modified ZnO nanorods. (b) J-V curves of PSCs based on ZnO nanorods with and without TiO_2 modification. (c) Schematic diagram of surface recombination suppression by Al_2O_3. (d) J-V curves of PSCs with cycles of ALD-Al_2O_3 on ZnO nanorods; inset: energy band diagram of the PSCs based on ZnO nanorods with Al_2O_3 coating. The XRD patterns and optical images of perovskite films deposited on (e) PCBM modified ZnO and (f) PEI modified ZnO during the annealing process. XRD patterns and optical images of perovskite on solution processed ZnO (g) without and (h) with 100 ºC annealing. (i) The optical images of perovskite films deposited on sputtered ZnO, sputtered Al doped ZnO (AZO) and sol-gel ZnO. (j) Lewis acid sites on the surface of the grains introduced by replacing

Zn with Al in AZO.

Surface passivation is an easy and efficient way to suppress the surface recombination, and researches has been carried out by many groups in this area. Son et al.[124] reported a solution method to fabricate a thin layer of TiO_2 on the surface of ZnO nanorods. The surface morphology of TiO_2 modified ZnO nanorods is shown in **Figure 7**(a). As shown in the figure, the ZnO surface is uniformly covered by TiO_2. The J-V curves of PSCs based on ZnO ETMs with and without TiO_2 modification are shown in Figure 7(b). As expected, the photovoltaic performance especially the Voc and FF increased by varying degrees, which indicates that the surface modification is an efficient method to suppress the surface recombination. Similar results are also reported by Dong et al.[155] and Chen et al.[156] Besides TiO_2, in 2016, our group modified the ZnO nanorods by an ultrathin Al_2O_3 film fabricated by the ALD method.[157, 158] After modification with the Al_2O_3 film, the PCE of PSC was improved from 11.72% of those without modification to 16.08%. Schematic diagram of surface recombination inhibition process is shown in Figure 7(c). As shown in the figure, the trap states originated from defects on ZnO surfaces capture the photon generated electrons and holes, which lead to the severe recombination. The Al_2O_3 modification suppresses the surface defects, improves the carrier extraction efficiency, and further improves the solar cell performance. Moreover, the thickness of Al_2O_3 has an important impact on solar cell performance. The thickness of ALD-Al_2O_3 films is controlled by the number of ALD cycles. The solar cell performance with different ALD cycles is shown in Figure 7(d). The figure displays that the best PCE is obtained with two ALD cycles of

Al_2O_3 films. This is because that one ALD cycle of the Al_2O_3 film can't form a continuous film, while three ALD cycles of Al_2O_3 film significantly increase the series resistance. Either a too thin or too thick Al_2O_3 film decreases the solar cell performance. Except the inorganic materials, segmented copolymers, like PCBM and poly(ethylene imine) (PEI),[152, 159] are also used to modify the interface of ZnO and perovskite. These materials usually have a more negative conduction band edge than that of ZnO. As a result, once ZnO surface is covered by these materials, the surface recombination sites are passivated and an energy barrier is formed to prevent the photon injected electrons from approaching the ZnO surface.[160] For these reasons, the surface recombination is efficiently suppressed.

Another widely used method in improving ZnO ETM quality is intentional doping. Dong et al. fabricated an ultrathin AZO (Al doped ZnO) film on the surface of ZnO nanorods by spin coating.[161] After Al doping, the electrical properties of ZnO, e.g. higher electron mobility, are significantly improved. In addition, Al doped ZnO has higher conduction band than ZnO. As a result, Al doping restrains the recombination at the ZnO/perovskite interface. Mahmood et al. fabricated electron rich nitrogen doped ZnO nanorods with a PEI capping layer on the surface. In their research, the ZnO nanorods was prepared with hydrothermal method. In order to achieve nitrogen doping, ammonium acetate was added into the ZnO nanorods growth solution. In addition, to suppress the surface recombination, the surface of ZnO nanorods was cover by PEI film. The PSC based on this modified ZnO nanorods yield a PCE of 16.1%.[159] Similar results can be obtained by Mg,[162, 163] Go,[164] Sn,[165-167] In [168] and Ni [169] doping.

As for the stability, the reduction of surface defects and surface passivation are effective for improving the stability of PSCs either. After surface passivation, the active ZnO surface is covered with TiO_2, PEI,[152] Al_2O_3, or other stabilized material, which have been proved not to react with perovskite films. As a result, the chemical instability induced by ZnO and chemical residues can also be avoided. Figure 7(e) and (f) exhibited the XRD patterns of perovskite film on PCBM and PEI modified ZnO films during annealing process. And the XRD patterns of perovskite on ZnO film without modification is shown in Figure 7(g). As can be seen, for unmodified ZnO, perovskite decompose rapidly after 30 min annealing. The perovskite on PCBM modified ZnO remain stable for the beginning 30 min and start to decompose as the time goes on. And the perovskite on PEI modified ZnO remain stable for the whole annealing process. The different stability between perovskite on PEI modified ZnO and PCBM modified ZnO is mainly because that the PCBM will aggregate under high temperature, as a result, the ZnO will contact with perovskite again.

It is worth noting that, the thickness of the passivation layer should be precisely controlled to avoid any negative effects, e.g. increase in series resistance. In addition, especially for solution processed ZnO ETMs, high temperature annealing is an efficient method, though not ideal in terms of energy consumption, to improve the stability of PSCs. Yang et al.[141] and Cheng et al.[152] reported improved stability of PSCs using this method. Figure 7(g) and (h) show the XRD patterns of perovskite films during annealing on different ZnO films. As shown in the figures, the perovskite on annealed ZnO demonstrate better stability. This is because that by high temperature annealing,

the surface hydroxyl groups and residual organic ligands, which are responsible for instability, decompose and volatilize. In addition, the perovskite film can remain stable on AZO films. Figure 7(i) shows the photos of perovskite films on ZnO film, AZO film prepared by RF sputtering and ZnO film prepared by sol-gel method. As can be seen, the perovskite on ZnO films prepared by RF sputtering method exhibited much higher thermal ability than perovskite on ZnO fabricated by sol-gel method. And the stability was furtherly improved by Al doping. The difference of stability between ZnO prepared by RF sputtering and sol-gel method is because that there are no chemical residues and less defects in ZnO prepared by RF sputtering. As for Al doping, according to Zhao et al.[170] and Tseng et al.[61, 171] the improved stability can be ascribed to the lower surface basicity of AZO films than that of pure ZnO films. Lewis acid sites are produced on the surface of the grains introduced by replacing Zn with Al in AZO, as shown in Figure 7(j). Overall, the two methods mentioned above can suppress the recombination and improve the stability simultaneously.

To sum up, the performance and structure of PSCs based on ZnO ETM from different fabrication processes are compared in **Table 1**. As can be seen, the best performing PSC based on ZnO ETM shows a PCE of 17.6% and RF sputtering method was used to fabricate the planar Al doped ZnO ETM. Another PSC with PCE over 17% is based on the Al_2O_3 modified ZnO nanorods, which is prepared by the hydrothermal method and modified by ALD. Therefore, the fabrication method and surface morphology of ZnO ETM are not the only determinant factors for high performance of PSCs. Additionally, by comparing the performance of PSCs based on the ZnO ETM

Table 1. The overview of PSCs based on ZnO ETM with different morphologies.

Morphology of ZnO	Method	Structure	Jsc (mA/cm^2)	Voc(V)	FF(%)	PCE(%)	Ref.
Compact layer	RF Sputtering	ITO/ZnO/$MAPbI_3$/spiro-OMeTAD/Ag	19.9	1.1	0.65	13.9	172
Compact layer	Self-Assemble	ITO/ZnO/C3-SAM/$MAPbI_3$/spiro-OMeTAD/MoO_3/Ag	22.5	1.1	0.65	15.7	173
Compact layer	nanoparticle	FTO/ZnO/$MAPbI_3$/C	20	0.8	0.54	8.7	116
Compact layer	nanoparticle	PEN/ITO/ZnO/$MAPbI_3$/C	13.4	0.8	0.42	4.3	116
Compact layer	nanoparticle	PET/ITO/ZnO/$MAPbI_3$/spiro-OMeTAD/Ag	13.4	1	0.74	10.2	3
Compact layer	nanoparticle	ITO/ZnO/$MAPbI_3$/spiro-OMeTAD/Ag	20.4	1	0.75	15.7	3
Compact layer	ALD	FTO/ZnO/mp-Al_2O_3-$MAPbI_3$/spiro-OMeTAD/Ag	20.4	1	0.66	13.1	93
Compact layer	chemical bath deposition	FTO/bl-ZnO/$MAPbI_3$/spiro-OMeTAD/Au	11.3	1.1	0.45	5.5	174
Compact layer	chemical bath deposition	PET/ITO/bl-ZnO/$MAPbI_3$/spiro-OMeTAD/Au	5.6	1	0.4	2.2	174
Compact layer	electrochemical	ITO/ZnO/$MAPbI_3$/spiro-OMeTAD/Ag	23.1	0.9	0.5	10.3	175
Compact layer	electrospraying	FTO/ZnO/$MAPbI_3$/spiro-OMeTAD/Ag	16	1	0.67	10.8	94
Compact layer	electrospraying	FTO/AZO/$MAPbI_3$/spiro-OMeTAD/Ag	15.1	1.1	0.76	12	94
Compact layer	Sol-gel	ITO/ZnO/PCBM/$MAPbI_3$/PTB7-Th/MnO_x/Ag	14.7	1	0.73	11	176
Compact layer	Sol-gel	ITO/ZnO/$MAPbI_3$/spiro-OMeTAD/MnO_x/Ag	18.2	1	0.67	12.2	176
Compact layer	chemical bath deposition	FTO/bl-ZnO/$MAPbI_3$/spiro-OMeTAD/Au	17	1	0.51	8.9	174
Compact layer	sol-gel	FTO/bl-ZnO/$MAPbI_3$/spiro-OMeTAD/Au	17.4	1	0.67	11.4	141
Compact layer	sol-gel	FTO/Annealed-bl-ZnO/$MAPbI_3$/spiro-OMeTAD/Au	17.4	1	0.47	7.9	141
Compact layer	sol-gel	FTO/bl-ZnO/$MAPbI_3$/spiro-OMeTAD/Au	7.3	0.8	0.48	2.9	152
Compact layer	sol-gel	FTO/bl-ZnO/$MAPbI_3$/spiro-OMeTAD/Au	13.7	0.8	0.494	5.4	152
Compact layer	sol-gel	FTO/bl-ZnO/PEI/$MAPbI_3$/spiro-OMeTAD/Au	16.8	0.9	0.69	10.2	152
Compact layer	sol-gel	FTO/bl-ZnO/PCBM/$MAPbI_3$/spiro-OMeTAD/Au	16	0.9	0.46	6.4	152
Compact layer	chemical bath deposition	PET/ITO/bl-ZnO/mp-ZnO-$MAPbI_3$/spiro-OMeTAD/Au	7.5	0.8	0.43	2.6	174
Compact layer	RF Sputtering	AZO/$MAPbI_3$/spiro-OMeTAD/Au	20.2	0.9	0.67	12.6	170
Compact layer	RF Sputtering	ITO/AZO/$MAPbI_3$/spiro-OMeTAD	21.7	1.1	0.756	17.6	61
Compact layer	ALD	FTO/ZnO/mp-Al_2O_3/$MAPbI_3$/spiro-OMeTAD	18.9	1	0.62	15.55	177
Nanorods	RF Sputtering	ITO/ZnO/$MAPbI_3$/spiro-OMeTAD/MoO_3/Ag	22.4	1	0.57	13.4	178
Nanorods	Hydrothermal	FTO/bl-ZnO/mp-ZnO/AZO shell/$MAPbI_3$/spiro-OMeTAD/Au	19.8	0.9	0.6	10.7	161
Nanorods	Hydrothermal	FTO/bl-ZnO/mp-ZnO-$MAPbI_3$/spiro-OMeTAD/Au	20.1	1	0.56	11.1	119
Nanorods	Hydrothermal	FTO/bl-ZnO/mp-ZnO-$MAPbI_3$/spiro-OMeTAD/Au	21.39	0.7	0.43	6.63	125
Nanorods	Hydrothermal	FTO/bl-ZnO/mp-ZnO/Al_2O_3/$MAPbI_3$/spiro-OMeTAD/Au	22.42	1	0.71	16.08	158
Nanorods	Hydrothermal	FTO/bl-ZnO/mp-ZnO/Al_2O_3/$MAPbI_3$/spiro-OMeTAD/Au	20.9	1.1	0.78	17.3	127
Nanorods	Hydrothermal	FTO/bl-ZnO/mp-ZnO/$MAPbI_3$/spiro-OMeTAD/Au	20.4	1	0.599	11.68	124
Nanorods	Hydrothermal	FTO/bl-ZnO/mp-ZnO/TiO_2/$MAPbI_3$/spiro-OMeTAD/Au	19.44	1.1	0.698	14.35	124
Nanorods	Hydrothermal	FTO/bl-ZnO/N doped ZnO/PEI/$MAPbI_3$/spiro-OMeTAD/Au	21.5	1	0.7	16.12	159
Nanowalls	Hydrothermal	FTO/ZnO nanowall/$MAPbI_3$/spiro-OMeTAD/Au	18.9	1	0.721	13.6	130
QDs	Hydrothermal	FTO/ZnO/$MAPbI_3$/spiro-OMeTAD/Au	15.1	0.9	0.53	7.5	179
QDs	Hydrothermal	FTO/ZnO/Graphene/$MAPbI_3$/spiro-OMeTAD/Au	21.7	1	0.68	15.2	179
QDs	Hydrothermal	PET/FTO/ZnO/Graphene/$MAPbI_3$/spiro-OMeTAD/Au	20.9	0.9	0.6	11.2	179
QDs	Hydrothermal	PET/ITO/Graphene/ZnO/$MAPbI_3$/spiro-OMeTAD/Au	16.8	0.9	0.62	9.73	137

and the AZO ETM (both prepared by RF sputtering), we can find that the Al doping can efficiently improve the performance the PSCs. Similar trend can also be found between the PSCs based on ZnO nanorods with and without surface modification. As a result, optimization of PSCs should not be restricted to only the ZnO ETM but should also be applied to the properties of interface and other layers. Nonetheless, PSCs based on ZnO materials have made great progress, and a great deal of efforts have been made to solve the instability and serious recombination induced by the ZnO ETM, which are the main reasons for the inferior performance of ZnO ETM based PSCs compared with their TiO_2 counterparts. Through the modification of ZnO ETM, the performance of PSCs based on the ZnO ETM is further improved. Although remarkable results have been achieved, some issues yet to be addressed, e.g. long-term stability, and researches on the ZnO ETM and the optimization of PSCs based on the ZnO ETM have to be carried on.[172-179]

7. Summary

In the last few years, the performance of PSCs have made great progress. Many fabrication methods and new perovskite compounds have been developed to fabricate high performance solar cells. As a powerful alternative to the widely used TiO_2 ETMs, ZnO materials share similar physical properties to TiO_2 but with much higher electron mobility. In addition, there are many simpler methods to fabricate ZnO nanomaterials with low cost and energy consumption. In this article, we briefly introduced different preparation methods of ZnO materials used in PSCs and review the development history of PSCs based on ZnO ETMs. Since ZnO ETMs was first used in PSCs, the

PCE of PSCs based on ZnO ETMs have been boosted from 5.0% to over 17%. Besides the high performance, ZnO nanomaterials are used to fabricate flexible devices, benefited from the rich varieties of fabrication methods. This is another distinct advantage compared to TiO_2 ETMs.

Compared with the PSCs based on TiO_2 ETMs, the performance of ZnO ETM based solar cells is still inferior. This is mainly caused by the serious surface recombination, high defect density, and poor stability. Many researches have been carried out to address these issues in the last couple of years and a number of plausible solutions have been proposed and demonstrated. The future researches on ZnO ETM based PSCs will continue to compete with their TiO_2 counterparts. It may still be the main focus to optimize the material quality of ZnO ETMs and hence to reduce the recombination and improve charge collections. The long term stability of ZnO ETM based perovskite solar cell is another important problem that must be solved in the next a few years. Nonetheless, with all that, ZnO-based perovskite solar cells have achieved a striking success as their TiO_2 counterparts and the march for next generation high efficient and low cost photovoltaic technology still continues.

Acknowledgements

This work was supported by National Natural Science Foundation of China under Grant Nos. 61421002，61574029, 61371046 and 61474015. This work was also partially supported by University of Kentucky.

References

[1] M. Liu, M. B. Johnston, H. J. Snaith, *Nature* **2013**, *501*, 395.

[2] N. J. Jeon, J. H. Noh, Y. C. Kim, W. S. Yang, S. Ryu, S. I. Seok, *Nat. Mater.* **2014**, *13*, 897.

[3] D. Liu, T. L. Kelly, *Nat. Photonics* **2013**, *8*, 133.

[4] F. Hong, B. Saparov, W. Meng, Z. Xiao, D. B. Mitzi, Y. Yan, *J. Phys. Chem. C* **2016**, *120*, 6435.

[5] B. Saparov, J.-P. Sun, W. Meng, Z. Xiao, H.-S. Duan, O. Gunawan, D. Shin, I. G. Hill, Y. Yan, D. B. Mitzi, *Chem. Mater.* **2016**, *28*, 2315.

[6] Z. Xiao, W. Meng, J. Wang, Y. Yan, *ChemSusChem* **2016**, *9*, 2628.

[7] Z. Xiao, W. Meng, J. Wang, D. B. Mitzi, Y. Yan, *Mater. Horiz.* **2017**, *4*, 206.

[8] Z. Xiao, W. Meng, B. Saparov, H. S. Duan, C. Wang, C. Feng, W. Liao, W. Ke, D. Zhao, J. Wang, D. B. Mitzi, Y. Yan, *J. Phys. Chem. Lett.* **2016**, *7*, 1213.

[9] Y. Yu, C. Wang, C. R. Grice, N. Shrestha, D. Zhao, W. Liao, L. Guan, R. A. Awni, W. Meng, A. J. Cimaroli, K. Zhu, R. J. Ellingson, Y. Yan, *ACS Energy Lett.* **2017**, *2*, 1177.

[10] W. Liao, D. Zhao, Y. Yu, C. R. Grice, C. Wang, A. J. Cimaroli, P. Schulz, W. Meng, K. Zhu, R. G. Xiong, Y. Yan, *Adv. Mater.* **2016**, *28*, 9333.

[11] M. A. Green, A. Ho-Baillie, H. J. Snaith, *Nat. Photonics* **2014**, *8*, 506.

[12] M. Gratzel, *Nat. Mater.* **2014**, *13*, 838.

[13] G. Li, R. Zhu, Y. Yang, *Nat. Photonics* **2012**, *6*, 153.

[14] M. M. Lee, J. Teuscher, T. Miyasaka, T. N. Murakami, H. J. Snaith, *Science* **2012**,

338, 643.

[15] G. Xing, N. Mathews, S. Sun, S. S. Lim, Y. M. Lam, M. Grätzel, S. Mhaisalkar, T. C. Sum, *Science* **2013**, *342*, 344.

[16] S. D. Stranks, G. E. Eperon, G. Grancini, C. Menelaou, M. J. Alcocer, T. Leijtens, L. M. Herz, A. Petrozza, H. J. Snaith, *Science* **2013**, *342*, 341.

[17] D. B. Mitzi, *J. Chem. Soc., Dalton Trans.* **2001**, *0*, 1.

[18] C. C. Stoumpos, C. D. Malliakas, M. G. Kanatzidis, *Inorg. Chem.* **2013**, *52*, 9019.

[19] D. H. Kim, J. Park, Z. Li, M. Yang, J. S. Park, I. J. Park, J. Y. Kim, J. J. Berry, G. Rumbles, K. Zhu, *Adv. Mater.* **2017**, *29*, 1606831.

[20] M. N. Hoque, N. Islam, Z. Li, G. Ren, K. Zhu, Z. Fan, *ChemSusChem* **2016**, *9*, 2692.

[21] S. Collavini, S. F. Völker, J. L. Delgado, *Angew. Chem., Int. Ed.* **2015**, *54*, 9757.

[22] A. Kojima, K. Teshima, Y. Shirai, T. Miyasaka, *J. Am. Chem. Soc.* **2009**, *131*, 6050.

[23] J. H. Im, C. R. Lee, J. W. Lee, S. W. Park, N. G. Park, *Nanoscale* **2011**, *3*, 4088.

[24] H. S. Kim, C. R. Lee, J. H. Im, K. B. Lee, T. Moehl, A. Marchioro, S. J. Moon, R. Humphry-Baker, J. H. Yum, J. E. Moser, M. Gratzel, N. G. Park, *Sci. Rep.* **2012**, *2*, 591.

[25] J. Burschka, N. Pellet, S. J. Moon, R. Humphry-Baker, P. Gao, M. K. Nazeeruddin, M. Gratzel, *Nature* **2013**, *499*, 316.

[26] H. Zhou, Q. Chen, G. Li, S. Luo, T. B. Song, H. S. Duan, Z. Hong, J. You, Y. Liu, Y. Yang, *Science* **2014**, *345*, 542.

[27] S. Pang, H. Hu, J. Zhang, S. Lv, Y. Yu, F. Wei, T. Qin, H. Xu, Z. Liu, G. Cui, *Chem. Mater.* **2014**, *26*, 1485.

[28] N. J. Jeon, J. H. Noh, W. S. Yang, Y. C. Kim, S. Ryu, J. Seo, S. I. Seok, *Nature* **2015**, *517*, 476.

[29] T. M. Koh, K. Fu, Y. Fang, S. Chen, T. C. Sum, N. Mathews, S. G. Mhaisalkar, P. P. Boix, T. Baikie, *J. Phys. Chem. C* **2014**, *118*, 16458.

[30] X. Zheng, C. Wu, S. K. Jha, Z. Li, K. Zhu, S. Priya, *ACS Energy Lett.* **2016**, *1*, 1014.

[31] Z. Wang, Y. Zhou, S. Pang, Z. Xiao, J. Zhang, W. Chai, H. Xu, Z. Liu, N. P. Padture, G. Cui, *Chem. Mater.* **2015**, *27*, 7149.

[32] D. Zhao, Y. Yu, C. Wang, W. Liao, N. Shrestha, C. R. Grice, A. J. Cimaroli, L. Guan, R. J. Ellingson, K. Zhu, X. Zhao, R.-G. Xiong, Y. Yan, *Nat. Energy* **2017**, *2*, 17018.

[33] W. Liao, D. Zhao, Y. Yu, N. Shrestha, K. Ghimire, C. R. Grice, C. Wang, Y. Xiao, A. J. Cimaroli, R. J. Ellingson, N. J. Podraza, K. Zhu, R. G. Xiong, Y. Yan, *J. Am. Chem. Soc.* **2016**, *138*, 12360.

[34] Y. Yu, C. Wang, C. R. Grice, N. Shrestha, J. Chen, D. Zhao, W. Liao, A. J. Cimaroli, P. J. Roland, R. J. Ellingson, *ChemSusChem* **2016**, *9*, 3288.

[35] W. S. Yang, J. H. Noh, N. J. Jeon, Y. C. Kim, S. Ryu, J. Seo, S. I. Seok, *Science* **2015**, *348*, 1234.

[36] D. Bi, W. Tress, M. I. Dar, P. Gao, J. Luo, C. Renevier, K. Schenk, A. Abate, F. Giordano, J. P. Correa Baena, J. D. Decoppet, S. M. Zakeeruddin, M. K. Nazeeruddin, M. Gratzel, A. Hagfeldt, *Sci. Adv.* **2016**, *2*, e1501170.

[37] M. Saliba, T. Matsui, J. Y. Seo, K. Domanski, J. P. Correa-Baena, M. K.

Nazeeruddin, S. M. Zakeeruddin, W. Tress, A. Abate, A. Hagfeldt, M. Gratzel, *Energy Environ Sci* **2016**, *9*, 1989.

[38] W. S. Yang, B.-W. Park, E. H. Jung, N. J. Jeon, Y. C. Kim, D. U. Lee, S. S. Shin, J. Seo, E. K. Kim, J. H. Noh, *Science* **2017**, *356*, 1376.

[39] C.-C. Chueh, C.-Z. Li, A. K. Y. Jen, *Energy Environ. Sci.* **2015**, *8*, 1160.

[40] H. S. Jung, N. G. Park, *Small* **2015**, *11*, 10.

[41] J. You, L. Meng, T.-B. Song, T.-F. Guo, Y. Yang, W.-H. Chang, Z. Hong, H. Chen, H. Zhou, Q. Chen, Y. Liu, N. De Marco, Y. Yang, *Nat. Nanotechnol.* **2015**, *11*, 75.

[42] J. You, Z. Hong, Y. M. Yang, Q. Chen, M. Cai, T.-B. Song, C.-C. Chen, S. Lu, Y. Liu, H. Zhou, *ACS nano* **2014**, *8*, 6.

[43] H. Xi, S. Tang, X. Ma, J. Chang, D. Chen, Z. Lin, P. Zhong, H. Wang, C. Zhang, *ACS Omega* **2017**, *2*, 326.

[44] Z. Lin, J. Chang, J. Xiao, H. Zhu, Q.-H. Xu, C. Zhang, J. Ouyang, Y. Hao, *Sol. Energy Mater. Sol. Cells* **2016**, *157*, 783.

[45] J. Huang, K.-X. Wang, J.-J. Chang, Y.-Y. Jiang, Q.-S. Xiao, Y. Li, *J. Mater. Chem. A* **2017**, *5*, 13817.

[46] H. Yang, J. Zhang, C. Zhang, J. Chang, Z. Lin, D. Chen, X. Sun, H. Xi, G. Han, Y. Hao, *Sol. Energy* **2016**, *139*, 190.

[47] J. Mo, C. Zhang, J. Chang, H. Yang, H. Xi, D. Chen, Z. Lin, G. Lu, J. Zhang, Y. Hao, *J. Mater. Chem. A* **2017**, *5*, 13032.

[48] S. Pang, D. Chen, C. Zhang, J. Chang, Z. Lin, H. Yang, X. Sun, J. Mo, H. Xi, G. Han, J. Zhang, Y. Hao, *Sol. Energy Mater. Sol. Cells* **2017**, *170*, 278.

[49] W. Yu, K. Wang, B. Guo, X. Qiu, Y. Hao, J. Chang, Y. Li, *J. Power Sources* **2017**, *358*, 29.

[50] R. Sandoval‐Torrientes, J. Pascual, I. García‐Benito, S. Collavini, I. Kosta, R. Tena‐Zaera, N. Martín, J. L. Delgado, *ChemSusChem* **2017**, *10*, 2023.

[51] S. Collavini, I. Kosta, S. F. Völker, G. Cabanero, H. J. Grande, R. Tena‐Zaera, J. L. Delgado, *ChemSusChem* **2016**, *9*, 1263.

[52] J. Pascual, I. Kosta, T. Tuyen Ngo, A. Chuvilin, G. Cabanero, H. J. Grande, E. M. Barea, I. Mora‐Seró, J. L. Delgado, R. Tena‐Zaera, *ChemSusChem* **2016**, *9*, 2679.

[53] P. Docampo, J. M. Ball, M. Darwich, G. E. Eperon, H. J. Snaith, *Nat. Commun.* **2013**, *4*, 2761.

[54] C.-G. Wu, C.-H. Chiang, Z.-L. Tseng, M. K. Nazeeruddin, A. Hagfeldt, M. Grätzel, *Energy Environ. Sci.* **2015**, *8*, 2725.

[55] C.-H. Chiang, M. K. Nazeeruddin, M. Grätzel, C.-G. Wu, *Energy Environ. Sci.* **2017**, *10*, 808.

[56] J. H. Heo, H. J. Han, D. Kim, T. K. Ahn, S. H. Im, *Energy Environ. Sci.* **2015**, *8*, 1602.

[57] K. Tokunaga, Hydrogenation of Fullerene C60: Material Design of Organic Semiconductors by Computation[M]. InTech: Croatia, **2012**.

[58] N. K. Elumalai, M. A. Mahmud, D. Wang, A. Uddin, *Energies* **2016**, *9*, 861.

[59] L.-C. Chen, J.-R. Wu, Z.-L. Tseng, C.-C. Chen, S. H. Chang, J.-K. Huang, K.-L. Lee, H.-M. Cheng, *Materials* **2016**, *9*, 747.

[60] Q. Bao, X. Liu, S. Braun, M. Fahlman, *Adv. Energy Mater.* **2014**, *4*, 1301272.

[61] Z.-L. Tseng, C.-H. Chiang, S.-H. Chang, C.-G. Wu, *Nano Energy* **2016**, *28*, 311.

[62] Q. Zhang, C. S. Dandeneau, X. Zhou, G. Cao, *Adv. Mater.* **2009**, *21*, 4087.

[63] Z. L. Wang, *J. Phys.: Condens. Matter* **2004**, *16*, R829.

[64] H. Liu, Z. Huang, S. Wei, L. Zheng, L. Xiao, Q. Gong, *Nanoscale* **2016**, *8*, 6209.

[65] L. Vayssieres, *Adv. Mater.* **2003**, *15*, 464.

[66] Y. Li, G. Meng, L. Zhang, F. Phillipp, *Appl. Phys. Lett.* **2000**, *76*, 2011.

[67] Y. Kong, D. Yu, B. Zhang, W. Fang, S. Feng, *Appl. Phys. Lett.* **2001**, *78*, 407.

[68] Y. Xing, Z. Xi, Z. Xue, X. Zhang, J. Song, R. Wang, J. Xu, Y. Song, S. Zhang, D. Yu, *Appl. Phys. Lett.* **2003**, *83*, 1689.

[69] Y. Sun, G. M. Fuge, N. A. Fox, D. J. Riley, M. N. Ashfold, *Adv. Mater.* **2005**, *17*, 2477.

[70] Z. W. Pan, Z. R. Dai, Z. L. Wang, *Science* **2001**, *291*, 1947.

[71] X. Bai, P. Gao, Z. L. Wang, E. Wang, *Appl. Phys. Lett.* **2003**, *82*, 4806.

[72] C. Ronning, P. Gao, Y. Ding, Z. L. Wang, D. Schwen, *Appl. Phys. Lett.* **2004**, *84*, 783.

[73] W. L. Hughes, Z. L. Wang, *Appl. Phys. Lett.* **2005**, *86*, 043106.

[74] Y. Ding, X. Y. Kong, Z. L. Wang, *Phys. Rev. B* **2004**, *70*, 235408.

[75] Z. Tu, Q. Li, X. Hu, *Phys. Rev. B* **2006**, *73*, 115402.

[76] Y. Wang, X. Li, N. Wang, X. Quan, Y. Chen, *Sep. Purif. Technol.* **2008**, *62*, 727.

[77] B. Fang, C. Zhang, W. Zhang, G. Wang, *Electrochim. Acta* **2009**, *55*, 178.

[78] Y.-J. Kim, J. Yoo, B.-H. Kwon, Y. J. Hong, C.-H. Lee, G.-C. Yi, *Nanotechnology* **2008**, *19*, 315202.

[79] C. Pacholski, A. Kornowski, H. Weller, *Angew. Chem., Int. Ed.* **2002**, *41*, 1188.

[80] X. Wang, C. J. Summers, Z. L. Wang, *Nano Lett.* **2004**, *4*, 423.

[81] P. Carcia, R. McLean, M. Reilly, G. Nunes Jr, *Appl. Phys. Lett.* **2003**, *82*, 1117.

[82] K. H. Kim, K. C. Park, D. Y. Ma, *J. Appl. Phys.* **1997**, *81*, 7764.

[83] Z. L. Tseng, C. H. Chiang, C. G. Wu, *Sci. Rep.* **2015**, *5*, 13211.

[84] Ü. Özgür, Y. I. Alivov, C. Liu, A. Teke, M. Reshchikov, S. Doğan, V. Avrutin, S.-J. Cho, H. Morkoc, *J. Appl. Phys.* **2005**, *98*, 11.

[85] H. J. Snaith, A. Abate, J. M. Ball, G. E. Eperon, T. Leijtens, N. K. Noel, S. D. Stranks, J. T.-W. Wang, K. Wojciechowski, W. Zhang, *J. Phys. Chem. Lett.* **2014**, *5*, 1511.

[86] V. Miikkulainen, M. Leskelä, M. Ritala, R. L. Puurunen, *J. Appl. Phys* **2013**, *113*, 2.

[87] D. Kim, H. Kang, J.-M. Kim, H. Kim, *Appl. Surf. Sci.* **2011**, *257*, 3776.

[88] B. Sang, A. Yamada, M. Konagai, *Jpn. J. Appl. Phys.* **1998**, *37*, L206.

[89] S. Berg, L. Andersson, H. Norström, E. Grusell, *Vacuum* **1977**, *27*, 189.

[90] S. M. Sultan, K. Sun, O. Clark, T. B. Masaud, Q. Fang, R. Gunn, J. Partridge, M. Allen, P. Ashburn, H. Chong, *IEEE Electron Device Lett.* **2012**, *33*, 203.

[91] T. Tynell, M. Karppinen, *Semicond. Sci. Technol.* **2014**, *29*, 043001.

[92] K.-M. Lee, S. H. Chang, K.-H. Wang, C.-M. Chang, H.-M. Cheng, C.-C. Kei, Z.-L. Tseng, C.-G. Wu, *Sol. Energy* **2015**, *120*, 117.

[93] X. Dong, H. Hu, B. Lin, J. Ding, N. Yuan, *Chem. Commun.* **2014**, *50*, 14405.

[94] K. Mahmood, B. S. Swain, H. S. Jung, *Nanoscale* **2014**, *6*, 9127.

[95] Z. Li, C. Xiao, Y. Yang, S. P. Harvey, D. H. Kim, J. A. Christians, M. Yang, P. Schulz, S. U. Nanayakkara, C.-S. Jiang, J. M. Luther, J. J. Berry, M. C. Beard, M. M. Al-Jassim, K. Zhu, *Energy Environ. Sci.* **2017**, *10*, 1234.

[96] C. Wang, C. Xiao, Y. Yu, D. Zhao, R. A. Awni, C. R. Grice, K. Ghimire, D. Constantinou, W. Liao, A. J. Cimaroli, P. Liu, J. Chen, N. J. Podraza, C.-S. Jiang, M. M. Al-Jassim, X. Zhao, Y. Yan, *Adv. Energy Mater.* **2017**, 1700414.

[97] C. Wang, D. Zhao, Y. Yu, N. Shrestha, C. R. Grice, W. Liao, A. J. Cimaroli, J. Chen, R. J. Ellingson, X. Zhao, Y. Yan, *Nano Energy* **2017**, *35*, 223.

[98] W. Ke, C. Xiao, C. Wang, B. Saparov, H. S. Duan, D. Zhao, Z. Xiao, P. Schulz, S. P. Harvey, W. Liao, W. Meng, Y. Yu, A. J. Cimaroli, C. S. Jiang, K. Zhu, M. Al-Jassim, G. Fang, D. B. Mitzi, Y. Yan, *Adv. Mater.* **2016**, *28*, 5214.

[99] W. Tress, *J. Phys. Chem. Lett.* **2017**, *8*, 3106.

[100] N.-G. Park, T. Miyasaka, M. Grätzel, Organic-Inorganic Halide Perovskite Photovoltaics[M]. Springer: Cham, Switzerland, **2016**.

[101] J. Shi, X. Xu, D. Li, Q. Meng, *Small* **2015**, *11*, 2472.

[102] H.-S. Kim, I. Mora-Sero, V. Gonzalez-Pedro, F. Fabregat-Santiago, E. J. Juarez-Perez, N.-G. Park, J. Bisquert, *Nat. Commun.* **2013**, *4*, 2242.

[103] Y. Sun, J. H. Seo, C. J. Takacs, J. Seifter, A. J. Heeger, *Adv. Mater.* **2011**, *23*, 1679.

[104] E. A. Meulenkamp, *J. Phys. Chem. B* **1998**, *102*, 5566.

[105] H. Zeng, W. Cai, P. Liu, X. Xu, H. Zhou, C. Klingshirn, H. Kalt, *ACS nano* **2008**, *2*, 1661.

[106] H. Zeng, G. Duan, Y. Li, S. Yang, X. Xu, W. Cai, *Adv. Funct. Mater.* **2010**, *20*, 561.

[107] X. Zhang, Y. Li, J. Zhao, S. Wang, Y. Li, H. Dai, X. Sun, *J. Power Sources* **2014**, *269*, 466.

[108] M. Ahmad, E. Ahmed, Y. Zhang, N. Khalid, J. Xu, M. Ullah, Z. Hong, *Curr. Appl. Phys.* **2013**, *13*, 697.

[109] W. J. Beek, M. M. Wienk, R. A. Janssen, *Adv. Funct. Mater.* **2006**, *16*, 1112.

[110] W. J. Beek, M. M. Wienk, R. A. Janssen, *Adv. Mater.* **2004**, *16*, 1009.

[111] T. P. Chou, Q. Zhang, G. E. Fryxell, G. Cao, *Adv. Mater.* **2007**, *19*, 2588.

[112] R. Zhang, C. Fei, B. Li, H. Fu, J. Tian, G. Cao, *ACS Appl. Mater. Interfaces* **2017**, *9*, 9785.

[113] M. Dürr, A. Schmid, M. Obermaier, S. Rosselli, A. Yasuda, G. Nelles, *Nat. Mater.* **2005**, *4*, 607.

[114] J. T. Wang, J. M. Ball, E. M. Barea, A. Abate, J. A. Alexander-Webber, J. Huang, M. Saliba, I. Mora-Sero, J. Bisquert, H. J. Snaith, R. J. Nicholas, *Nano Lett.* **2014**, *14*, 724.

[115] K. Hwang, Y. S. Jung, Y. J. Heo, F. H. Scholes, S. E. Watkins, J. Subbiah, D. J. Jones, D. Y. Kim, D. Vak, *Adv. Mater.* **2015**, *27*, 1241.

[116] H. Zhou, Y. Shi, K. Wang, Q. Dong, X. Bai, Y. Xing, Y. Du, T. Ma, *J. Phys. Chem. C* **2015**, *119*, 4600.

[117] R. Viswanatha, H. Amenitsch, D. Sarma, *J. Am. Chem. Soc.* **2007**, *129*, 4470.

[118] D. Bi, G. Boschloo, S. Schwarzmuller, L. Yang, E. M. Johansson, A. Hagfeldt,

Nanoscale **2013**, *5*, 11686.

[119] D.-Y. Son, J.-H. Im, H.-S. Kim, N.-G. Park, *J. Phys. Chem. C* **2014**, *118*, 16567.

[120] J. H. Im, I. H. Jang, N. Pellet, M. Gratzel, N. G. Park, *Nat. Nanotechnol.* **2014**, *9*, 927.

[121] L.-W. Ji, S.-M. Peng, J.-S. Wu, W.-S. Shih, C.-Z. Wu, I.-T. Tang, *J. Phys. Chem. Solids* **2009**, *70*, 1359.

[122] J. H. Noh, S. W. Lee, *Electron. Mater. Lett.* **2008**, *4*, 71.

[123] L. Whittaker-Brooks, J. M. Mativetsky, A. Woll, D. Smilgies, Y.-L. Loo, *Org. Electron.* **2013**, *14*, 3477.

[124] D.-Y. Son, K.-H. Bae, H.-S. Kim, N.-G. Park, *J. Phys. Chem. C* **2015**, *119*, 10321.

[125] M. Wang, S. Li, P. Zhang, Y. Wang, H. Li, Z. Chen, *Chem. Phys. Lett.* **2015**, *639*, 283.

[126] M. Yang, Z. Li, M. O. Reese, O. G. Reid, D. H. Kim, S. Siol, T. R. Klein, Y. Yan, J. J. Berry, M. F. A. M. van Hest, K. Zhu, *Nat. Energy* **2017**, *2*, 17038.

[127] S. Li, P. Zhang, H. Chen, Y. Wang, D. Liu, J. Wu, H. Sarvari, Z. D. Chen, *J. Power Sources* **2017**, *342*, 990.

[128] M. Yang, Y. Zeng, Z. Li, D. H. Kim, C. S. Jiang, J. van de Lagemaat, K. Zhu, *Phys. Chem. Chem. Phys.* **2017**, *19*, 5043.

[129] M. Yang, T. Zhang, P. Schulz, Z. Li, G. Li, D. H. Kim, N. Guo, J. J. Berry, K. Zhu, Y. Zhao, *Nat. Commun.* **2016**, *7*, 12305.

[130] J.-F. Tang, Z.-L. Tseng, L.-C. Chen, S.-Y. Chu, *Sol. Energy Mater. Sol. Cells*

2016, *154*, 18.

[131] M. Law, L. E. Greene, J. C. Johnson, R. Saykally, P. Yang, *Nat. Mater.* **2005**, *4*, 455.

[132] G. Hu, W. Guo, R. Yu, X. Yang, R. Zhou, C. Pan, Z. L. Wang, *Nano Energy* **2016**, *23*, 27.

[133] G. Zhu, Y. Zhou, S. Wang, R. Yang, Y. Ding, X. Wang, Y. Bando, Z. lin Wang, *Nanotechnology* **2012**, *23*, 055604.

[134] G. Rani, P. Sahare, *J. Mater. Sci. Technol.* **2013**, *29*, 1035.

[135] L. Xie, Y. Wang, H. Zhang, *Appl. Phys. Lett.* **2009**, *94*, 061905.

[136] K. Deng, T. Gong, L. Hu, X. Wei, Y. Chen, M. Yin, *Opt. Express* **2011**, *19*, 1749.

[137] S. Ameen, M. S. Akhtar, H.-K. Seo, M. K. Nazeeruddin, H.-S. Shin, *J. Phys. Chem. C* **2015**, *119*, 10379.

[138] A. Janotti, C. G. Van de Walle, *Rep. Prog. Phys.* **2009**, *72*, 126501.

[139] F. Oba, S. R. Nishitani, S. Isotani, H. Adachi, I. Tanaka, *J. Appl. Phys.* **2001**, *90*, 824.

[140] A. Kohan, G. Ceder, D. Morgan, C. G. Van de Walle, *Phys. Rev. B* **2000**, *61*, 15019.

[141] J. Yang, B. D. Siempelkamp, E. Mosconi, F. De Angelis, T. L. Kelly, *Chem. Mater.* **2015**, *27*, 4229.

[142] S. Chen, C. E. Small, C. M. Amb, J. Subbiah, T. h. Lai, S. W. Tsang, J. R. Manders, J. R. Reynolds, F. So, *Adv. Energy Mater.* **2012**, *2*, 1333.

[143] L. J. Brillson, Y. Lu, *J. Appl. Phys.* **2011**, *109*, 8.

[144] L. Brillson, H. Mosbacker, M. Hetzer, Y. Strzhemechny, G. Jessen, D. Look, G. Cantwell, J. Zhang, J. Song, *Appl. Phys. Lett.* **2007**, *90*, 102116.

[145] L.-L. Yang, Q. Zhao, M. Willander, X. Liu, M. Fahlman, J. Yang, *Appl. Surf. Sci.* **2010**, *256*, 3592.

[146] Q. Zhao, L.-L. Yang, M. Willander, B. E. Sernelius, P. Holtz, *J. Appl. Phys.* **2008**, *104*, 073526.

[147] D. P. McMeekin, G. Sadoughi, W. Rehman, G. E. Eperon, M. Saliba, M. T. Horantner, A. Haghighirad, N. Sakai, L. Korte, B. Rech, M. B. Johnston, L. M. Herz, H. J. Snaith, *Science* **2016**, *351*, 151.

[148] Y. Li, J. K. Cooper, W. Liu, C. M. Sutter-Fella, M. Amani, J. W. Beeman, A. Javey, J. W. Ager, Y. Liu, F. M. Toma, I. D. Sharp, *Nat. Commun.* **2016**, *7*, 12446.

[149] X. Li, D. Bi, C. Yi, J. D. Decoppet, J. Luo, S. M. Zakeeruddin, A. Hagfeldt, M. Gratzel, *Science* **2016**, *353*, 58.

[150] F. J. Ramos, M. C. López‐Santos, E. Guillén, M. K. Nazeeruddin, M. Grätzel, A. R. Gonzalez‐Elipe, S. Ahmad, *ChemPhysChem* **2014**, *15*, 1148.

[151] J. Yang, T. L. Kelly, *Inorg. Chem.* **2017**, *56*, 92.

[152] Y. Cheng, Q. D. Yang, J. Xiao, Q. Xue, H. W. Li, Z. Guan, H. L. Yip, S. W. Tsang, *ACS Appl. Mater. Interfaces* **2015**, *7*, 19986.

[153] P. Zhang, J. Wu, Y. Wang, H. Sarvari, D. Liu, Z. D. Chen, S. Li, *J. Mater. Chem. A* **2017**, *5*, 17368.

[154] A. G. Aberle, *Prog Photovoltaics /progress in photovoltaics* **2000**, *8*, 473.

[155] J. Dong, X. Xu, J.-J. Shi, D.-M. Li, Y.-H. Luo, Q.-B. Meng, Q. Chen, *Chin. Phys. Lett.* **2015**, *32*, 078401.

[156] P. Chen, X. Yin, M. Que, Y. Yang, W. Que, *RSC Advances* **2016**, *6*, 57996.

[157] S. Li, D. Liu, P. Zhang, Y. Wang, H. Sarvari, Y. Xuan, Z. D. Chen, *ECS Trans.* **2016**, *72*, 275.

[158] S. Li, P. Zhang, Y. Wang, H. Sarvari, D. Liu, J. Wu, Y. Yang, Z. Wang, Z. D. Chen, *Nano Res.* **2017**, *10*, 1092

[159] K. Mahmood, B. S. Swain, A. Amassian, *Adv. Energy Mater.* **2015**, *5*, 1500568.

[160] M. Law, L. E. Greene, A. Radenovic, T. Kuykendall, J. Liphardt, P. Yang, *J. Phys. Chem. B* **2006**, *110*, 22652.

[161] J. Dong, Y. Zhao, J. Shi, H. Wei, J. Xiao, X. Xu, J. Luo, J. Xu, D. Li, Y. Luo, Q. Meng, *Chem. Commun.* **2014**, *50*, 13381.

[162] J. Song, E. Zheng, L. Liu, X. F. Wang, G. Chen, W. Tian, T. Miyasaka, *ChemSusChem* **2016**, *9*, 2640.

[163] J. Dong, J. Shi, D. Li, Y. Luo, Q. Meng, *Appl. Phys. Lett.* **2015**, *107*, 073507.

[164] M. I. Ahmed, Z. Hussain, M. Mujahid, A. N. Khan, S. S. Javaid, A. Habib, *AIP Advances* **2016**, *6*, 065303.

[165] L. S. Oh, D. H. Kim, J. A. Lee, S. S. Shin, J.-W. Lee, I. J. Park, M. J. Ko, N.-G. Park, S. G. Pyo, K. S. Hong, J. Y. Kim, *J. Phys. Chem. C* **2014**, *118*, 22991.

[166] S. S. Shin, W. S. Yang, J. H. Noh, J. H. Suk, N. J. Jeon, J. H. Park, J. S. Kim, W. M. Seong, S. I. Seok, *Nat. Commun.* **2015**, *6*, 7410.

[167] S. S. Mali, C. S. Shim, H. Kim, C. K. Hong, *J. Mater. Chem. A* **2016**, *4*, 12158.

[168] J. Werner, G. Dubuis, A. Walter, P. Löper, S.-J. Moon, S. Nicolay, M. Morales-Masis, S. De Wolf, B. Niesen, C. Ballif, *Sol. Energy Mater. Sol. Cells* **2015**, *141*, 407.

[169] P.-Y. Chen, S.-H. Yang, *Opt. Mater. Express* **2016**, *6*, 3651.

[170] X. Zhao, H. Shen, Y. Zhang, X. Li, X. Zhao, M. Tai, J. Li, J. Li, X. Li, H. Lin, *ACS Appl. Mater. Interfaces* **2016**, *8*, 7826.

[171] A. Mekki-Berrada, D. Grondin, S. Bennici, A. Auroux, *Phys. Chem. Chem. Phys.* **2012**, *14*, 4155.

[172] J. Song, J. Bian, E. Zheng, X.-F. Wang, W. Tian, T. Miyasaka, *Chem. Lett.* **2015**, *44*, 610.

[173] L. Zuo, Z. Gu, T. Ye, W. Fu, G. Wu, H. Li, H. Chen, *J. Am. Chem. Soc.* **2015**, *137*, 2674.

[174] M. H. Kumar, N. Yantara, S. Dharani, M. Graetzel, S. Mhaisalkar, P. P. Boix, N. Mathews, *Chem. Commun.* **2013**, *49*, 11089.

[175] J. Zhang, T. Pauporté, *J. Phys. Chem. C* **2015**, *119*, 14919.

[176] J. Kim, G. Kim, T. K. Kim, S. Kwon, H. Back, J. Lee, S. H. Lee, H. Kang, K. Lee, *J. Mater. Chem. A* **2014**, *2*, 17291.

[177] H. Si, Q. Liao, Z. Zhang, Y. Li, X. Yang, G. Zhang, Z. Kang, Y. Zhang, *Nano Energy* **2016**, *22*, 223.

[178] L. Liang, Z. Huang, L. Cai, W. Chen, B. Wang, K. Chen, H. Bai, Q. Tian, B. Fan, *ACS Appl. Mater. Interfaces* **2014**, *6*, 20585.

[179] M. M. Tavakoli, R. Tavakoli, Z. Nourbakhsh, A. Waleed, U. S. Virk, Z. Fan, *Adv. Mater. Interfaces* **2016**, *3*, 1500790.